Cells
Tissues
Organs

Tissue Engineering – Regenerative Medicine/Research Article

Cells Tissues Organs 2025;214:219–241
DOI: 10.1159/000541524

Received: June 14, 2024
Accepted: September 6, 2024
Published online: October 9, 2024

Cancer Epithelial Cells Participate in the Self-Organization of Lung Tumor Spheroids: A Morphological Approach

Irene Monleón-Guinot[a, b] Lucía Bravo-Baranda[a, b] Lara Milián[a, b] María Sancho-Tello[a, b] Mauro Llop-Miguel[a] José Marcelo Galbis[c] Antonio Cremades[c] Carmen Carda[a, b, d] Manuel Mata[a, b, d]

[a]Department of Pathology, Faculty of Medicine and Dentistry, Universitat de València, Valencia, Spain; [b]INCLIVA Biomedical Research Institute, Valencia, Spain; [c]Hospital de la Ribera, Alzira, Valencia, Spain; [d]Biomedical Research Networking Center on Bioengineering, Biomaterials and Nanomedicina (CIBER-BBN), Madrid, Spain

Keywords
Lung cancer · Spheroids · 3D cell culture · Tumor microenvironment · Epithelial-to-mesenchymal transition

Abstract

Introduction/aims: The tumor microenvironment is known to play an important role in tumor progression. However, the specific mechanisms underlying this process are still not known in detail and more research is needed on the elements that control tumor progression in lung cancer. In this work, we aimed to investigate the involvement of epithelial and stromal cancer cells in growth, cell migration, and epithelial-to-mesenchymal transition (EMT) in a 3D in vitro model consisting of cell spheroids cultured in a type I collagen scaffold. ***Methods:*** Spheroids were manufactured using different combinations of epithelial cells, particularly H460 and H1792 cell lines, with cancer-associated fibroblasts and normal fibroblasts, both isolated from adenocarcinoma patients. We evaluated the morphology of the spheroids by analysis of F-actin and pankeratin with confocal microscopy. We determined the ultrastructure of cells in the spheroids by transmission electron microscopy and the expression of CDH1, CDH2, and VIM by RT-PCR. ***Results:*** We observed that, on the one hand, the type of epithelial cell influences the morphology of spheroids. Stromal cells stimulated spheroid growth and cell dissemination through the collagen matrix, either alone or organized in branches with a nucleus of epithelial cells preceded by fibroblast cells. They also induced the appearance of new cell groups in the scaffold and the presence of EMT markers. ***Conclusion:*** The results presented here indicate the participation of both epithelial and stromal cells in the control of spheroid self-organization. The experimental model proposed here, although preliminary, is useful for the study of some aspects related to tumor progression in lung cancer.

Irene Monleón-Guinot and Lucía Bravo-Baranda contributed equally to this work.

karger@karger.com
www.karger.com/cto

Correspondence to:
Manuel Mata, manuel.mata@uv.es

Plain Language Summary

Lung cancer remains a significant public health problem, causing millions of deaths each year, making it crucial to understand its complexities in order to developing effective therapeutic strategies. The tumor microenvironment, which refers to the environment surrounding a tumor and includes various cell types, signaling molecules, and the extracellular matrix, influences how the tumor grows and responds to treatments. This study investigates how different cells interact in lung cancer, using a 3D model that mimics cancer microenvironment. Spheroids of two types of lung cancer cells, H460 and H1792, with or without stromal cells were cultured in a collagen matrix, to study their behavior. The results showed that when cancer cell spheroids were cultured with stromal cells, the spheroids formed branches and the tumors grew larger. Gene expression analysis revealed that the cells were undergoing a process called EMT, associated with more aggressive tumor behavior. Detailed studies of cellular structure confirmed that stromal cells were causing significant changes in cancer cells. This model helps understand the progression of lung cancer and can be used to quickly test new drugs.

Introduction

Over the last decades, lung cancer has been one of the most diagnosed cancers, responsible for almost two million deaths per year, 20% of annual cancer deaths [1]. Prevention, early detection, comprehensive characterization, and personalized treatment are essential to reduce mortality from lung cancer. Lung cancer is classified into two main types: small cell lung cancer (SCLC) and non-small cell lung cancer (NSCLC). SCLC accounts for 15–20% of all lung cancers (often caused by smoking) and is characterized by a central tumor arising from the submucosa of the airways. On the other hand, NSCLC comprises the majority (around 80–85%) of lung cancer cases and includes several subtypes, such as adenocarcinoma, large-cell carcinoma, and squamous cell carcinoma. Additionally, bronchial carcinoid tumors are a less common subtype [2].

In NSCLC, the high metastatic capacity and the acquisition of resistance to treatments have been classically attributed to different mutations in key genes such as EGFR [3, 4] or BRAF [5], which are generated in specific clones of tumor cells. However, the acquisition of these mutations does not explain the enormous metastatic capacity of NSCLC, and therefore, other factors must be considered [5]. NSCLC tumors exhibit significant heterogeneity, encompassing not only tumor epithelial cells but also the vascularization, cancer-associated fibroblasts (CAFs), extracellular matrix (ECM), and infiltrating immune cells, as well as physical stimuli. The interactions between the different elements are what constitutes the so-called tumor microenvironment (TME). The biology of TME participates in key aspects in the pathophysiology of NSCLC, including metastasis or acquisition of resistance. Therefore, in recent years, the TME has become a priority objective for the identification of new biomarkers of the disease and even new pharmacological targets [5, 6].

The stroma of NSCLC is composed of a complex network of macromolecules that harbors different cell types, with type I collagen being the most abundant component [7, 8]. The tumor matrix differs considerably from normal lung matrix, which is rich in type III collagen and elastic fibers [9, 10]. Remodeling of the lung ECM is essential for tumor dissemination or metastasis and is carried out by specific cells in the TME that are the CAFs. CAFs are a heterogeneous population of cells of different origins, including normal stromal cells activated by adjacent cancer cells, tumor epithelial cells undergoing epithelial-to-mesenchymal transition (EMT), resident or circulating mesenchymal stem cells, or pericytes, among others [11].

EMT is an evolutionarily preserved developmental program, in which differentiated epithelial cells turn into mesenchymal cells. In this process, they lose both their polarity and their ability to adhere to other cell types. Tumor cells can use this program, which participates in carcinogenesis and confers them metastatic properties, improving the motility, invasiveness, and resistance to apoptotic stimuli of these cells [12].

The absence of study models that mimic the complexity of TME of NSCLC is a limiting factor in the understanding of its pathophysiology as well as in the development of new drugs for its treatment. Traditional in vitro models based in 2D cultures of standard cell lines have been widely used and have proven ineffective in clinical studies due to the inability of such cultures to faithfully reproduce the complexity of patients' tumors. Moreover, cancer cell lines generally do not maintain the genetic heterogeneity of the original tumors [13–15]. Regarding to, experimental animal models, although useful in preclinical investigation, are not without limitations [16].

For all these reasons, there is currently a need to develop new models for the study of NSCLC that better mimic its physiological conditions. There are numerous cancer research groups that are trying to generate 3D

study models that allow us to better address the interactions between different cell populations of the TME as well as control the elements of the ECM. Moreover, the possibility of obtaining primary cultures of tumor cells from patient should allow the manufacture of personalized models, which is in line with the goals of precision medicine [17, 18].

We have recently developed a study with a 3D model based on the culture of spheroids generated with both stromal cells from tumors of patients diagnosed with lung adenocarcinoma and the A549 cancer cell line, in a matrix composed of a type I collagen hydrogel. This model has allowed us to evaluate some aspects in relation to the self-organization of the lung tumor spheroids and cell dissemination through the matrix [19].

The aim of the present study was to advance the understanding of the interaction between the diverse types of cells included in our 3D culture model, in relation to cell growth, reorganization, and dissemination through the collagen hydrogel used. For this purpose, we have created spheroids by combining stromal cells from lung tumors of patients diagnosed with adenocarcinoma (CAFs) or from healthy peripheral tissue (normal fibroblasts [NFs]) obtained from the surgical resection area of the same patients, along with various cell lines of lung cancer. We have examined the morphology of the spheroids using immunofluorescence and electron microscopy techniques, and we have also analyzed molecular changes in the expression of relevant genes involved in the EMT process. The results presented in this study suggest that, in our model, both epithelial and stromal cancer cells collaborate in the self-organization of cellular aggregates and in the dissemination through the generated scaffold.

Methods

Cell Lines and Cell Isolation

Human lung NSCLC cell lines H460 and H1792 were purchased from the American Type Culture Collection (ATCC, Rockville, MD, USA). Both cell lines were cultured in Dulbecco's Modified Eagle Medium F12 (DMEM F12; Thermo Fisher Scientific Inc., Waltham, MA, USA) supplemented with 10% heat-inactivated fetal bovine serum (Gibco, Germany), 1% penicillin-streptomycin, and 1% amphotericin B (Euroclone, Siziano, PV, Italy) in a humidified atmosphere incubator at 37°C and 5% CO_2.

Stromal cells were isolated from lung adenocarcinoma from a patient undergoing surgery, as previously reported [20]. The tumor sample was collected at Hospital La Ribera in Alzira (Valencia, Spain). This study was conducted in accordance with the ethical standards outlined in the Declaration of Helsinki by the World Medical Association. All procedures included in this study were approved by the hospital Ethics Committee, and informed consent was obtained from all participating patients. The samples were collected between October and December 2023. To obtain CAFs and NFs, tumor and non-tumor tissues, respectively, were fragmented into small pieces of approximately 3 mm. These tissue fragments were then digested using DH liberase (Sigma-Aldrich, Madrid, Spain) for 90 min at 37°C with shaking. After digestion, the samples were filtered through a filter with 70 μm pores (Gibco, Madrid, Spain), washed with sterile phosphate-buffered saline (PBS, Sigma-Aldrich, Madrid, Spain), and cultured in fibroblast culture medium, containing high-glucose DMEM F12 supplemented with 10% heat-inactivated fetal bovine serum, 1% penicillin-streptomycin, and 1% amphotericin B. Cells were cultured in 6-well culture plates (Euroclone, Siziano PV, Italy) in an incubator until reaching confluence. Adherent cells were then expanded and subcultured for up to 6 passages [21].

Spheroid Formation

Spheroids were constructed using the hanging drop method. Cancer epithelial cells were cocultured with 50% or 70% stromal cells. The initial culture conditions were a concentration of 1.5×10^5 cells/mL and 72 h of hanging drop culture. They were then transferred to drops of type I collagen. The method used was optimized as previously described [19].

All cell types were expanded in 2D culture using supplemented DMEM F12 (see 4.1. Cell Lines and Cell Isolation). Fifty drops (25 μL/drop) of each cell suspension (1.5×10^5 cells/mL) were seeded on the inside of a Petri dish lid (87.8 mm diameter). The lids with the droplets were then quickly rotated to cover the Petri dish containing 8–10 mL of PBS, to maintain humidity inside the culture dish. The hanging droplets were incubated at 37°C and 5% CO_2 for 72 h.

After 72 h of incubation, the spheroids were collected with culture medium and transferred to a 15-mL conical tube (SPL Life Sciences, Korea). Due to gravity, all spheroids settled in approximately 10 min, allowing us to remove the supernatant. The pellet, containing the spheroids, was suspended in 450 μL of an ice-chilled solution containing 4 mg/mL rat type I collagen (Advanced BioMatrix, Carlsbad, CA, USA) and mixed with 50 μL of neutralizing solution (Advanced BioMatrix, Carlsbad, CA, USA). Drops of 20 μL were then

transferred to each well of 24-well untreated culture plate (Corning, ME, USA) and incubated for 30 min at 37°C to allow collagen to gel. Finally, the droplets were covered with culture medium. The culture medium was changed every 2–3 days. Spheroids were photographed daily for 1 week to study the evolution of cellular morphology, using a Leica DM IL LED phase contrast microscope (Leica Microsystems, Germany).

F-Actin Fluorescence Staining and Pankeratin Distribution by Immunofluorescence

F-actin microfilaments were evaluated using rhodamine-conjugated phalloidin (Molecular Probes, Thermo Fisher Scientific, Madrid, Spain) [22]. Cytokeratin was observed using pankeratin antibody (which reacts against peptides 4, 5, 6, 8, 10, 13, and 18). After being cultured for 1 week, spheroids were washed with PBS pH 7.4 and fixed in formalin for 30 min at 4°C. Once washed with PBS, the droplets were transferred either to 8-well MilliCell slides (Merck, Germany) or to µ-Slide 8 Well^{high} Glass Bottom chambered coverslips (ibidi, Gräfelfing, Germany) for visualization by epifluorescence or confocal microscopy, respectively. The spheroids were then permeabilized with 0.1% Triton X 100 in PBS for 5 min, and after two washes with PBS, samples were preincubated with PBS containing 1% BSA for 20 min to reduce the nonspecific background. Cells were then incubated with Cytokeratin Pan-Alexa fluor monoclonal primary antibody in 1:100 antibody diluent solution (Invitrogen, USA), overnight at 4°C. After two washes with PBS, each sample was stained for 60 min with phalloidin (1:400 dilution in PBS) and nuclei were stained with DAPI (1:100 dilution in PBS). Finally, samples were washed twice with PBS and analyzed with a Leica DM2500 Fluorescence Microscope (Leica, Wetzlar, Germany) or Leica TCS-SP8 Confocal Microscopy (Leica Corp., Madrid, Spain).

Transmission Electron Microscopy

A transmission electron microscopy (TEM) study was carried out to investigate the ultrastructure of the spheroids. After 1 week of spheroid culture, samples were washed with phosphate buffer (PB, Sorensen's PB) and fixed in 2.5% glutaraldehyde overnight at 4°C. Once washed with PB, spheroids were postfixed with 1% osmium tetroxide for 2 h at 4°C and dehydrated through a series of increasing concentrations of acetone, ending with 100% acetone + SO_4Cu. Finally, the samples were immersed in propylene oxide and then embedded in EPON epoxy resin and cut into ultrathin sections, which were double-stained with 3% uranyl acetate and lead citrate to improve contrast. Images of the ultrastructure were then captured using a transmission electron microscope (Hitachi 800, Japan).

Determination of CDH1, CDH2, and VIM Relative Expression Levels

Total RNA was extracted from spheroids after 1 week of culture, using the TRIzol reagent (ref.: 10296010, Thermo Fisher Scientific Inc., Waltham, MA, USA), according to the manufacturer's instructions. RNA concentration was determined by spectrophotometry using a NanoDrop 2000 Spectrophotometer (Fisher Scientific, Madrid, Spain).

Complementary DNA was synthesized using random primers (hexamers) and TaqMan RT reagents (Applied Biosystems, Foster City, CA, USA), according to the manufacturer's instructions. Reverse transcriptase polymerase chain reaction was performed to evaluate gene expression levels using High-Capacity cDNA Reverse Transcription Kit (ref.: 4368814, Applied Biosystems, Madrid, Spain) and the following probes: CDH1 (Hs01023894_m1), CDH2 (Hs00983056_m1), and VIM (Hs00958111_m1) (Thermo Fisher Scientific Inc., Waltham, MA, USA). The reactions were carried out in a 7900HT Real-Time Thermocycler (Applied Biosystems, Madrid, Spain). The comparative ΔΔCt method was used with glyceraldehyde 3-phosphate dehydrogenase (GAPDH: Mm99999915_g1) (Applied Biosystems, Madrid, Spain) as an endogenous control to determine the relative levels of gene expression. All reactions were performed in triplicate.

Morphometric Analysis

The 3D structure of the cultured spheroids was reconstructed from sequential images obtained by confocal microscopy (Leica TCS-SP8; Leica Corp., Madrid, Spain). The reconstruction process involved the use of the following parameters: a ×10 objective lens, and the number of z-stack steps set to half the optimal value suggested by the system. Videos were generated by compiling stacks of the acquired images using Imaris Microscopy Image Analysis Software, version 9.0 (Oxford Instruments, UK). The height of the spheroid in the Z plane was estimated by measuring the distance between the lowest and highest points of the spheroid, using the "draw scale bar" tool in the ZY orthogonal view.

Morphometric analysis was carried out as previously described, with minor modifications to adapt the methodology to the morphology of the generated organoids [23]. Sequential F-actin fluorescence-stained images were obtained by confocal microscopy. The

maximum projection of the branches and core of the spheroids were selected, and QuPath version 0.2.3 was used to analyze the data [24]. The level of the branches was considered as previously described [24]: level 1 branches are those that arise directly from the core of the spheroid, level 2 corresponds to the branches that arise from a level 1 branch, and so on. The following parameters were considered:

- Spheroid area: total area of the spheroid measured in the maximum projection image.
- Spheroid core: primary structure of the organoid from which branches arise.
- Branch area: stained area of branches connected to the core.
- Number of level 1 branches: number of branches that arise directly from the core of the spheroid.
- Number of level >1 branches: number of branches with a level higher than 1, that is, all those that originate from a branch. When there are more than 15 level 1 branches, we considered >15 due to the impossibility of measuring them. This occurs in those organoids with profuse branching.
- Level 1 branch length: average length of level 1 branches, measured from the base to the first ramification.
- Level 1 branch thickness: average thickness of level 1 branches, measured from their base.
- Maximum length of level 1 branches: measured from their base.
- Maximum thickness of level 1 branches: measured at their base.

Figure 1 shows an example of these measurements. All measurements were performed blind by three different investigators to ensure the objectivity of the results.

Data Presentation and Analysis

In this study, we have used stromal cells (CAFs and NFs) isolated from 5 different patients. All determinations have been carried out in triplicate. Quantitative data are shown as means ± SD and were subjected to ANOVA followed by Tukey's multiple-comparison test (GraphPad Software Inc., San Diego, CA, USA). Significance was accepted at $p < 0.05$.

Results

Spheroid Manufacture and Characterization

Spheroids from H460 and H1792 cell lines in combination or not with CAFs or NFs were generated using the hanging drop method (see "Material and Methods" section for details on spheroid formation). Both cell types were mixed at 50% of each, or at 30% epithelial cells and 70% of CAFs or NFs, at a density of 1.5×10^5 cells/mL and were observed every 24 h for 1 week to evaluate the evolution of their morphological by phase contrast microscopy. Representative results are shown in Figure 2. In addition, the area of these spheroids was calculated to improve the characterization (Fig. 3).

H460 cells formed spheroids that exhibited strong intercellular cohesion, resulting in compact structures. The spheroids were generated by combining two possible concentrations of H460 with NFs or with CAFs. When H460 and NFs were combined at 50%, spheroids were created that maintained the cohesion of the spheroids described above, and the appearance of some branching was also observed. When the percent of NFs was increased to 70%, the result was an increase in the size and number of the aforementioned branches. On the other hand, when H460 cells were combined with 50% or 70% CAFs, the appearance of a greater number of branches was observed than those observed with NFs but following the same branching pattern (Fig. 1a).

H1792 cells generated small, dispersed cell clusters that tended to branch through the collagen hydrogel. This behavior was accentuated when stromal cells, NFs, or CAFs were added, which resulted in a larger number of thick branches that occupied almost the entire scaffold, making it impossible to measure the areas. These effects were accentuated by increasing the percentage of stromal cells (from 50 to 70%) and were greater in the spheroids generated with CAFs compared to those generated with NFs (Fig. 1b).

Figure 3 summarizes the values of the area measurements of the H460 spheroids. As shown, the presence of NFs or CAFs remarkably increases the size of the generated spheroids compared to the initial spheroids. This effect was greater in spheroids generated with CAFs and was also depended on the initial proportion of stromal cells. Parallel to the growth of the spheroids, abundant branches appeared, the density of which made it impossible to reliably measure the area of the spheroids on day 7.

Fluorescence Microscope Evaluation of H460 Spheroids

The spheroids formed by the H460 cells presented clearly defined borders, with few migrating cells and relatively large size in most cases (Fig. 4a–c, online suppl. Video S1; for all online suppl. material, see https://doi.org/10.1159/000541524). The structure they generated was a multilayered sheet with spheric morphology, where

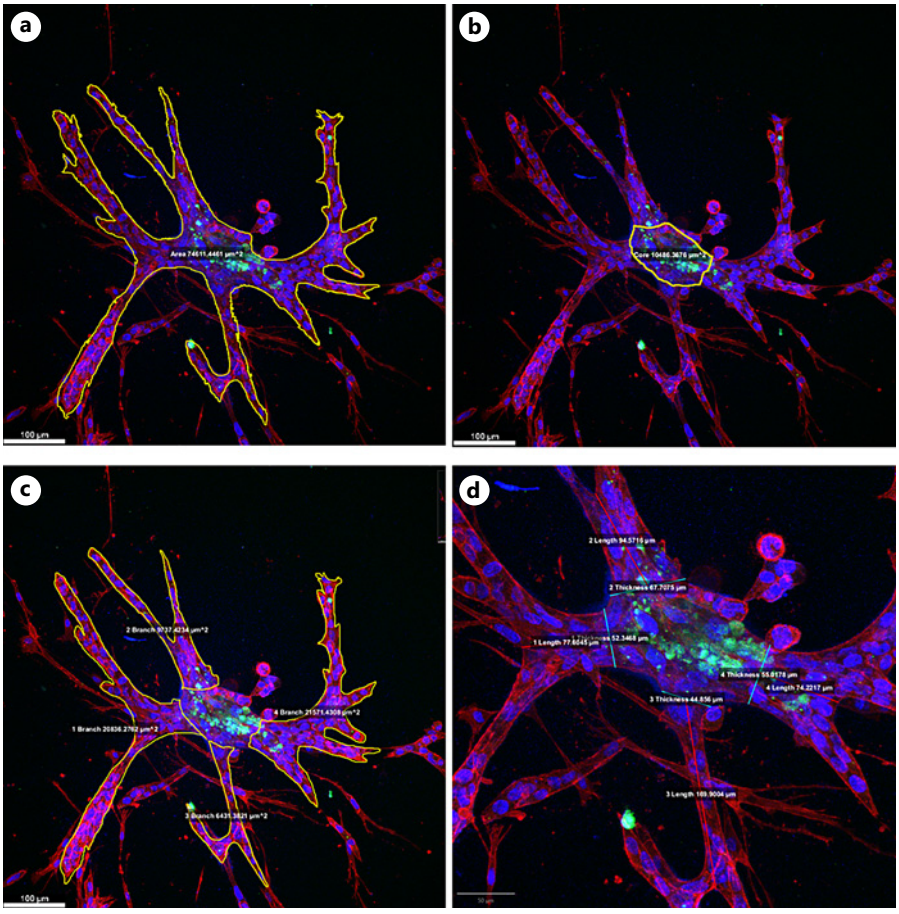

Fig. 1. Examples of morphometric evaluation of spheroids. **a** shows the area measurement of a spheroid generated with H1792 cells and NFs stained with rhodamine-conjugated phalloidin and studied with confocal microscopy. Only those branches that unambiguously connected to the core of the spheroid were selected after studying the sequential images generated with the confocal microscope. **b** shows the area measurement of the core area of this spheroid while (**c**) shows the measurement of the branch area. The measurement of the length and thickness of level one branches are shown in (**d**).

the fluorescence signal was not detected in the center. These structures appeared isolated or exceptionally forming large complex formed by adjacent cell groups (Fig. 4c). These spheroids were large and reached a height of 127 ± 25.8 μm in average (Fig. 4f). Regarding the morphology of the cells that make up the spheroids, those located in the inner surface of the multilayered sheet exhibited a characteristic epithelioid morphology, showing good intercellular cohesion and the expression of pankeratin (Fig. 4d). Furthermore, some smaller spheroids presumably formed by migrating cells from large spheroids were also observed. This small cell groups showed the same cohesion pattern, and cells were positive for pankeratin staining (Fig. 4e).

Fluorescence Microscope Evaluation of H460 + NF Spheroids

The incorporation of NFs into H460 spheroids generated notable changes in its morphology, which depended on the percentage of stromal cells added. In the spheroids generated with 50% tumor and 50% stromal cells, cells started to spread centrifugally from the compact structure, forming branches (Fig. 5a). Some larger spheroids appeared to form as a result of the fusion of some small spheroids in close proximity (Fig. 5b). In addition, the presence of fibroblasts seemed to have no discernible impact on the cohesion among epithelial cells (Fig. 5c).

The increase in the percent of stromal cells used to generate spheroids resulted in a notable increase in these changes. Complex structures apparently formed by the union of adjacent cell spheroids appeared (Fig. 6a, b, online suppl. Video S2). The size of the spheroids was larger, often greater than 300 μm (Fig. 6c). The main and central structure was large and well defined, formed by well-cohesive epithelial cells (Fig. 6d). Many fibroblastic cells emerge from the structure and appeared both isolated in the type I collagen matrix (Fig. 6b, e) and forming branches (Fig. 6f, g). These branches maintained a nucleus of epithelial cells closely united and positive for pankeratin (Fig. 6f). At the distal ends of these branches, fibroblastic cells were observed (Fig. 6g).

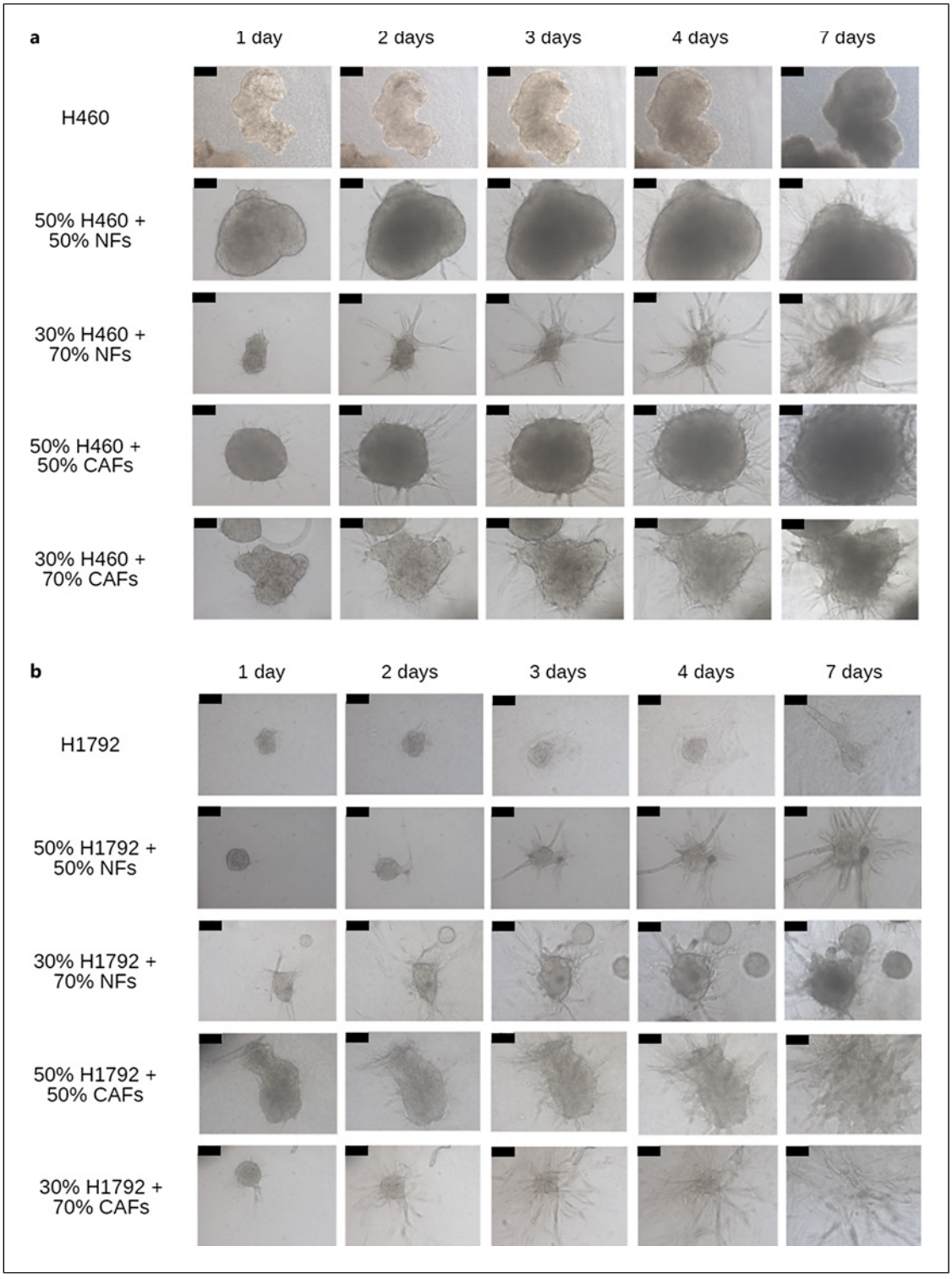

Fig. 2. Morphological evolution of spheroids. **a** Spheroids of H460 cells and spheroids of H460 cells + NFs or H460 cells + CAFs. **b** Spheroids of H1792 cells and spheroids of H1792 cells + NFs or H1792 + CAFs. In all cases, they were cultured for 1 week. Samples were observed using a phase contrast microscope. Representative images from $n = 5$ independent experiments. Scale bar (black bars) represents 100 μm.

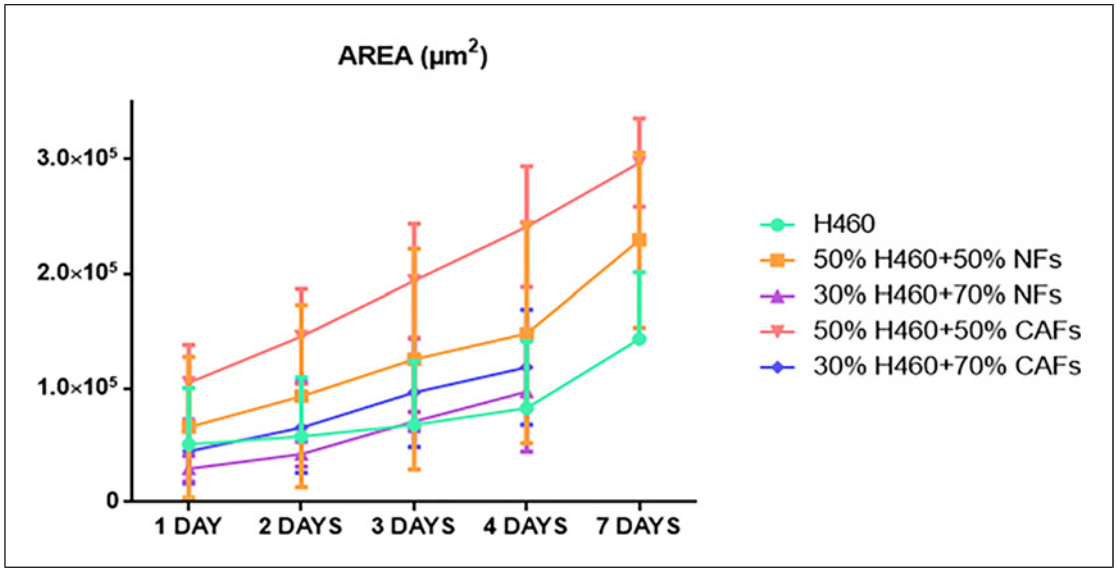

Fig. 3. Spheroid area. Spheroid areas were measured using ImageProPlus® 7.0 analytical software (Media Cybernetics Inc., Rockville, MD, USA). The mean area ± SD of $n = 5$ independent experiments. SD, standard deviation.

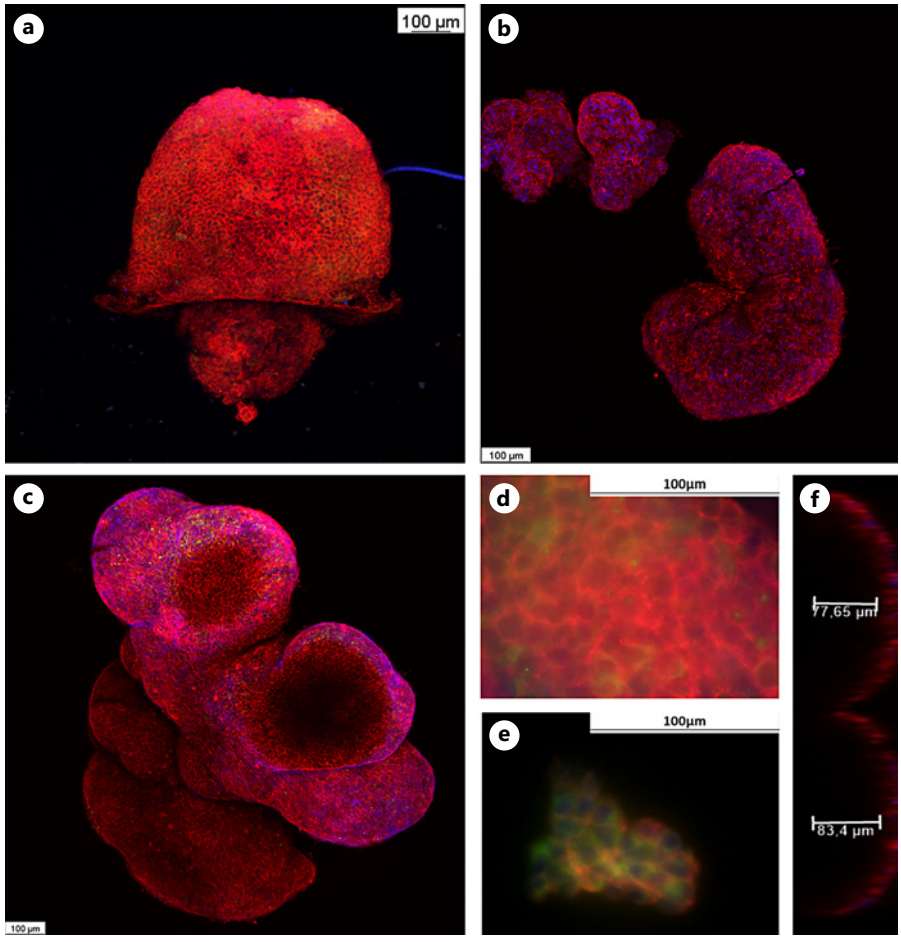

Fig. 4. Microscopic characterization of H460 spheroids. Spheroids were manufactured and cultured for 1 week. F-actin distribution was examined by phalloidin-rhodamine fluorescence staining (shown in red). Pankeratin expression was visualized by immunofluorescence staining (shown in green). Nuclei were stained with DAPI (shown in blue). Samples were observed with either a confocal (**a–c**, **f**) or epifluorescence microscope (**d**, **e**). The height of the spheroids was determined by confocal microscopy in the Z-axis (**f**). These results are representative of $n = 5$ different patients. Scale bar represents 100 μm.

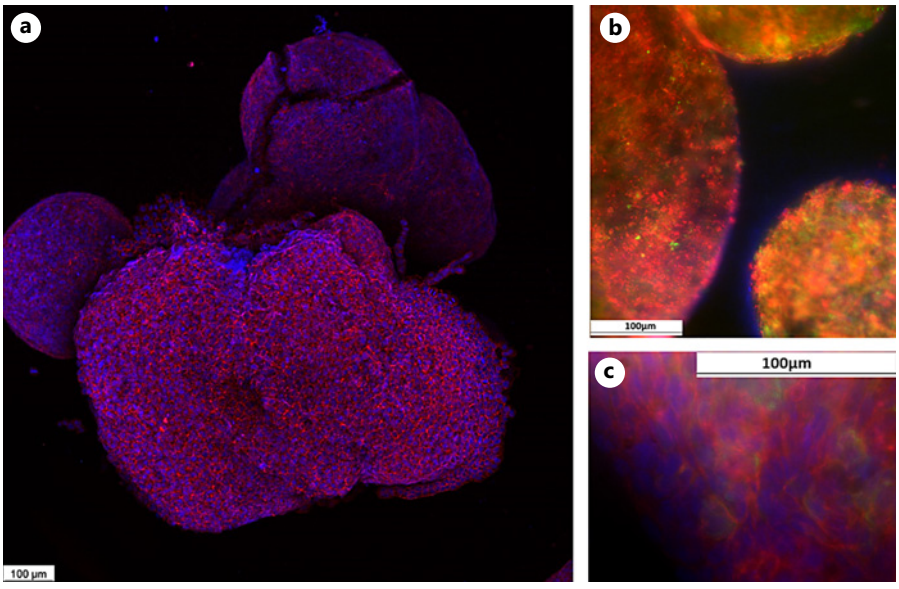

Fig. 5. Microscopic characterization of H460 + NF spheroids. The spheroids were manufactured and cultured for 1 week. An initial concentration of 50% stromal cells was used. F-actin distribution was examined by fluorescent staining with phalloidin-rhodamine (shown in red). Pankeratin expression was visualized by immunofluorescence staining (shown in green). Nuclei were stained with DAPI (shown in blue). Samples were observed either with a confocal (**a**) or epifluorescence microscope (**b**, **c**). The results presented are representative of $n = 5$. Scale bar represents 100 µm.

Fluorescence Microscope Evaluation of H460 + CAF Spheroids

Spheroids containing CAFs showed a large number of branches and a tendency to generate large-cell groups (Fig. 7a, 6e, online suppl. Video S3). We found larger structures when a higher percentage of CAFs was used (Fig. 7d, h). Despite the presence of CAFs, the spheroids maintained intercellular cohesion in both large (Fig. 7b) and smaller spheroids (Fig. 7f). Discrete groups of 2–3 epithelioid cells positive for pankeratin were found far from the spheroids (Fig. 7c). Several branches were observed in all the spheroids studied. These branches were composed of epithelial cells that maintain intercellular cohesion (Fig. 7g) and isolated migratory fibroblasts-like cells (pankeratin-negative) that could also be observed emerging from the spheroid (Fig. 7g). At the leading edge of the branches, cells with a fibroblastic phenotype that seemed to guide cell migration could be observed.

Morphometric Evaluation of H460 Spheroids

In order to study whether there were significant differences in relation to the size or branching of the spheroids, we performed a morphometric analysis as described in the Methods section. The results obtained are summarized in Figure 8 and show the comparison between spheroids formed with H460 cells and spheroids generated with H460 cells and 70% stromal cells (NFs or CAFs). According to microscope evaluation, we found an increase in the spheroid and core area in those spheroids containing stromal cells reaching statistical significance when H460 cells were combined with CAFs (Fig. 8a, b). We found an increase in the branching of the spheroids characterized by an increase in the area and quantity of branches, as well as in the length of the level one branches (Fig. 8c–g). Nevertheless, the thickness of the branches was not significantly changed (Fig. 8h, i).

Fluorescence Microscope Evaluation of H1792 Spheroids

The spheroids composed of the H1792 cell line did not form cohesive structures with well-defined edges (Fig. 9a, online suppl. Video S4). However, they formed dispersed structures scattered throughout the collagen scaffold. They tended to form epithelial layers that covered the matrix upon reaching the surface of the collagen drop (Fig. 9c). The height measured was lower than 80 µm (Fig. 9d). The cells formed epithelium-like structures, maintaining the intercellular junctions typical of epithelial cells (Fig. 9b). Cells starting to migrate from the epithelium generated branched structures due to the linear arrangement of epithelial cells (Fig. 9b).

Fluorescence Microscope Evaluation of 1792 + NF Spheroids

H1792 + NF spheroids showed a notable and ordered branching compared to H1792 spheroids (Fig. 9a), which became more dispersed when higher percentage of stromal cells was used (Fig. 10c, online suppl. Video S5). We observed the formation of small clusters of cells stained positively for pankeratin (Fig. 10b). Furthermore, numerous single cells migrated from the spheroid

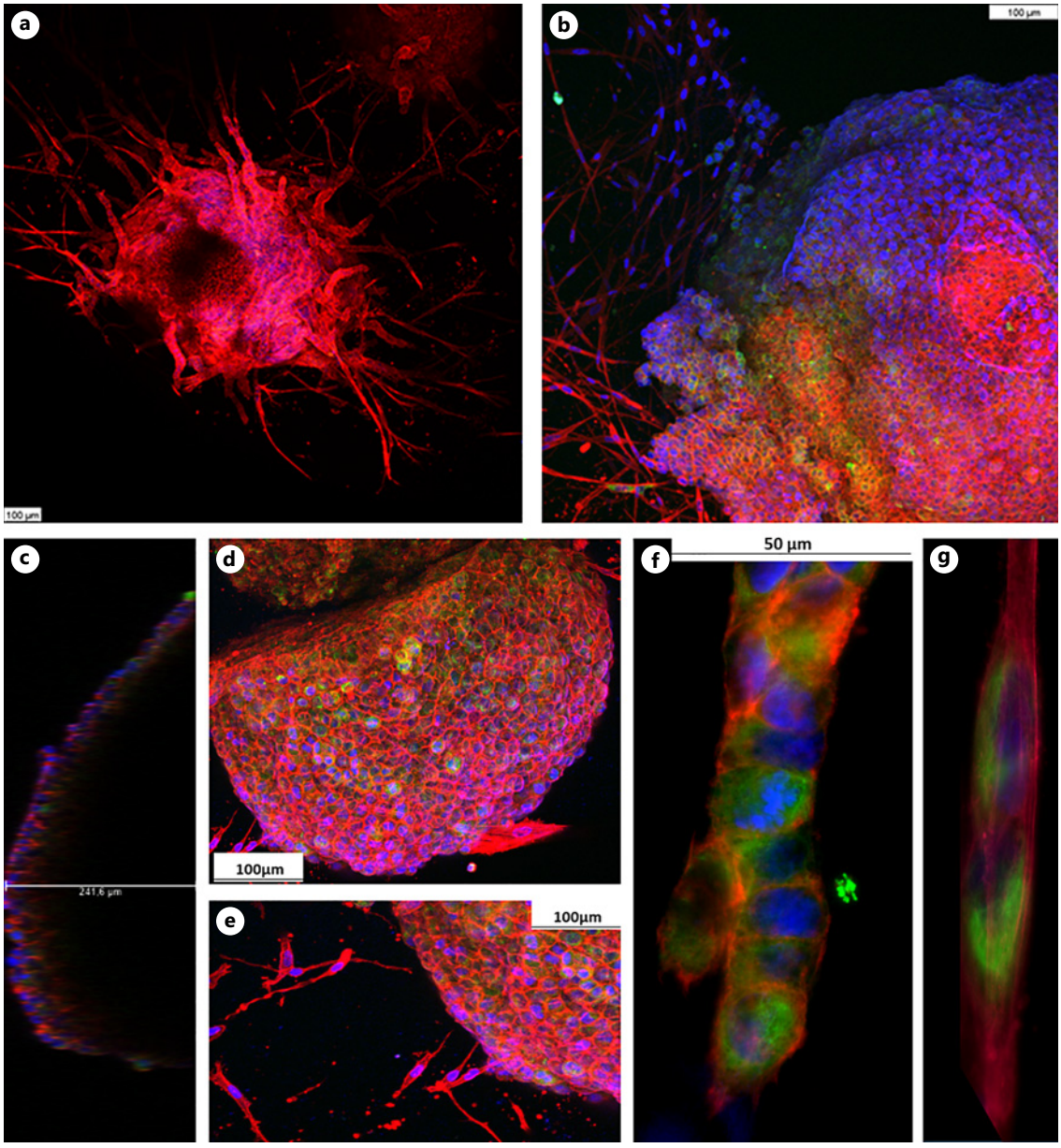

Fig. 6. Microscopic characterization of H460 + NF spheroids. The spheroids were manufactured and cultured for 1 week. An initial concentration of 70% stromal cells was used. F-actin distribution was examined by fluorescent staining with phalloidin-rhodamine (shown in red). Pankeratin expression was visualized by immunofluorescence staining (shown in green). Nuclei were stained with DAPI (shown in blue). Samples were observed either with a confocal (**a–e**) or epifluorescence microscope (**f**, **g**). The results presented are representative of $n = 5$.

without establishing connections with other cells (Fig. 10c). Numerous cells that migrated linearly and cohesively forming branches were observed. The higher the percentage of NFs used, the greater the number of and thinner branches were observed. These branches were formed by well-cohesive epithelioid cells in the spheroids manufactured with 50% NFs (Fig. 10d), while this cohesion pattern became more diffuse in the spheroids generated with 70% NFs. In this case, the branches were interspersed with fibroblastic cells that, in addition to preceding them, seemed to be included within them (Fig. 10e, f). They did not form large groups of cells, which did not allow us to measure the height of the spheroid.

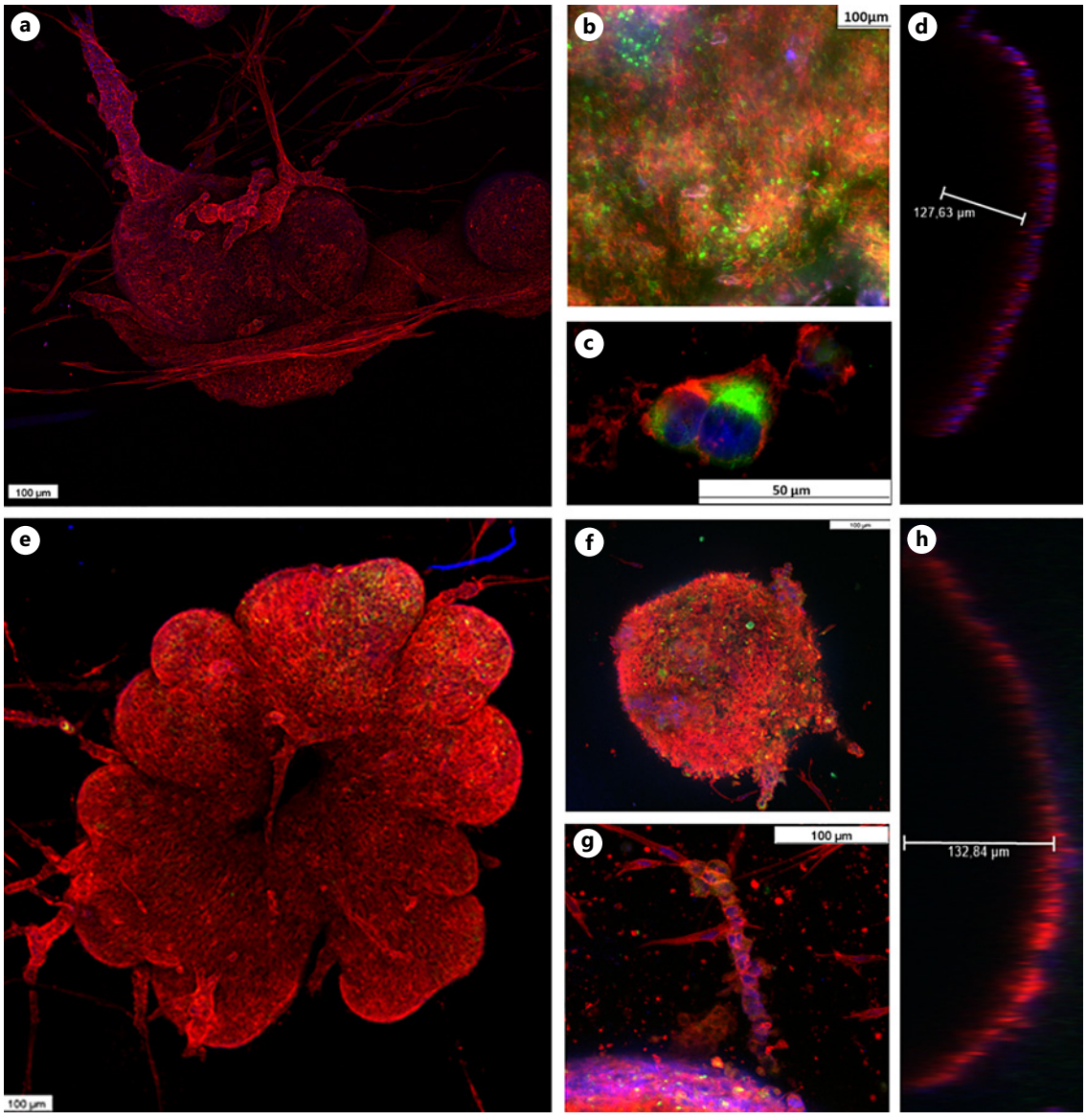

Fig. 7. Microscopic characterization of H460 + CAF spheroids. The spheroids were manufactured and cultured for 1 week. An initial percentage of 50% (**a–d**) or 70% (**e–h**) stromal cells was used. F-actin distribution was examined by fluorescence staining with phalloidin-rhodamine (shown in red). Pan-keratin expression was visualized by immunofluorescence staining (shown in green). Nuclei were stained with DAPI (shown in blue). Samples were observed with either a confocal (**a**, **d**, **e**, **f**, **h**) or epifluorescence microscope (**b**, **c**, **g**). The height of the spheroids was determined by confocal microscopy in the Z-axis (**d**, **h**). These results are representative of $n = 5$.

Fluorescence Microscope Evaluation of 1792 + CAF Spheroids

The organization pattern of the H1790 cells changed radically when CAFs were incorporated into the spheroids. The spheroids manufactured with 50% CAFs showed a very accentuated branching pattern. These branches appeared formed by very cohesive cells (Fig. 11a). Occasionally, the cells were organized in small pankeratin-positive groups (Fig. 11b). As the percent of CAFs increased, larger epithelial laminas positives for pankeratin (Fig. 11e, online suppl. Video S6) and more profuse, but less cohesive, branches appeared. Abundant fibroblastic cells not in contact with cell branches were found. These cells showed large pseudopods and cell extensions that spanned great distances (Fig. 11d, f).

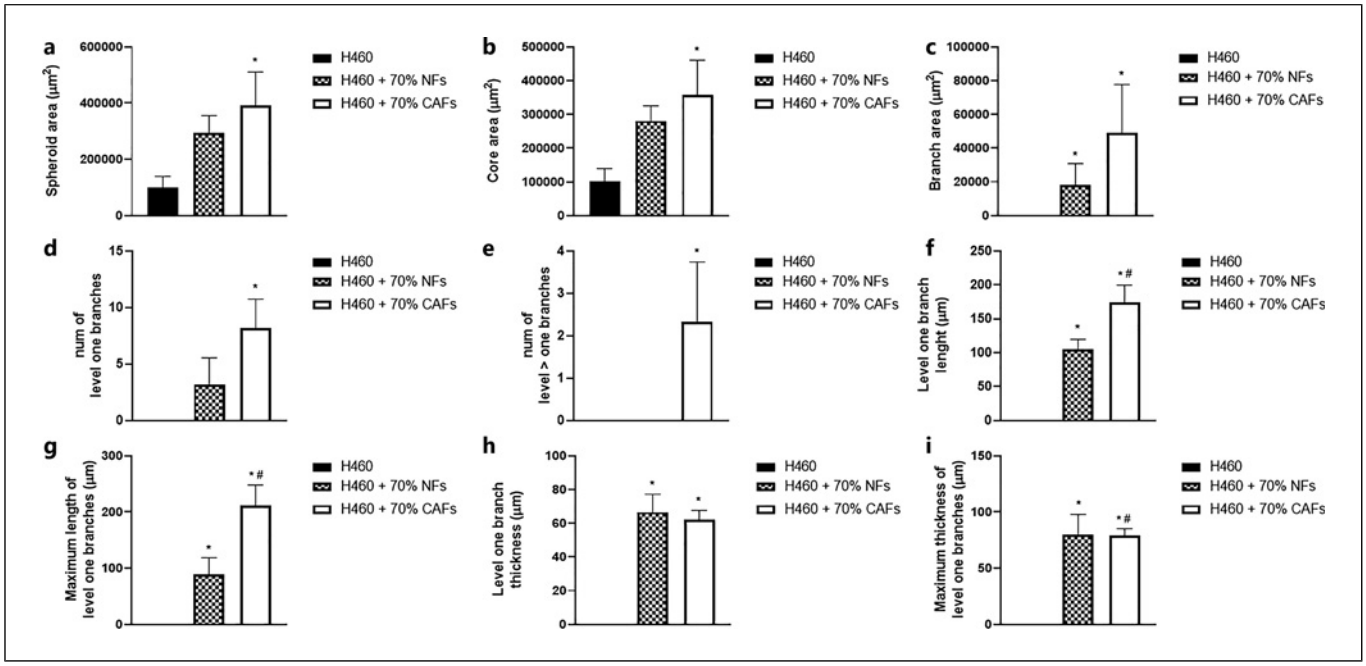

Fig. 8. a–i Morphometric evaluation of H460 spheroids. Spheroids were manufactured with or without stromal cells (NFs or CAFs) and cultured for 1 week. Morphometric evaluation was done. The results are represented as the mean ± SD of $n = 5$ independent experiments. Each condition was evaluated in 3–6 replicates from three independent observers in a blind manner. *$p < 0.05$ compared to H460 without stromal cell spheroids. #$p < 0.05$ compared to H460 + NF spheroids. SD, standard deviation.

Morphometric Evaluation of H1792 Spheroids

Morphometric analysis of H1792 cell spheroids was performed in the same manner as for H460 cell spheroids. Again, the results obtained supported the microscopic evaluation. Regarding the area of the spheroids, those generated with H1792 cells alone tended to form epithelioid structures, while the addition of stromal cells induced the appearance of branched structures, which explains the smaller area observed in the spheroids generated with cancer cells combined with NFs or CAFs (Fig. 12a). The core was difficult to estimate, due to the profuse branching of these spheroids. However, we did not find significant differences between the spheroids studied (Fig. 12b). The combination of H1792 cells with stromal cells generated profuse branching of the spheroids, notably increasing not only the area of the branches, but also the number of branches and the maximum length of the level 1 branches. These changes were, in general, more marked in the spheroids generated with H1792 cells and CAFs (Fig. 12c–g). No statistical differences according to the branch thickness were found (Fig. 12h, i).

Ultrastructural Features of Spheroids

An ultrastructural study of cell spheroids was performed using TEM. In spheroids, H460 cell showed a nucleus containing euchromatin, as well as the presence of a developed nucleolus (Fig. 13a). The epithelioid cells were attached by junctional complexes. In the periphery of the spheroid (Fig. 13b), abundant cellular processes of different sizes could be observed, of which the largest one could correspond to migratory cellular elements. Figure 13c shows a more panoramic image of the peripheral area of the spheroids, in which discrete deposits of ECM could be distinguished between the different processes observed.

Spheroids containing 70% NFs presented cells with a characteristic secretory phenotype (Fig. 14a). These cells exhibited a well-developed Golgi apparatus and numerous mitochondria with well-developed cristae. These cells showed low cohesion as they were not closely adhered to the spheroid. On the contrary, large intercellular spaces were observed, where deposits of ECM were found. At the periphery of the spheroid (Fig. 14b), numerous cells with elongated morphology and multiple processes could be observed, along with

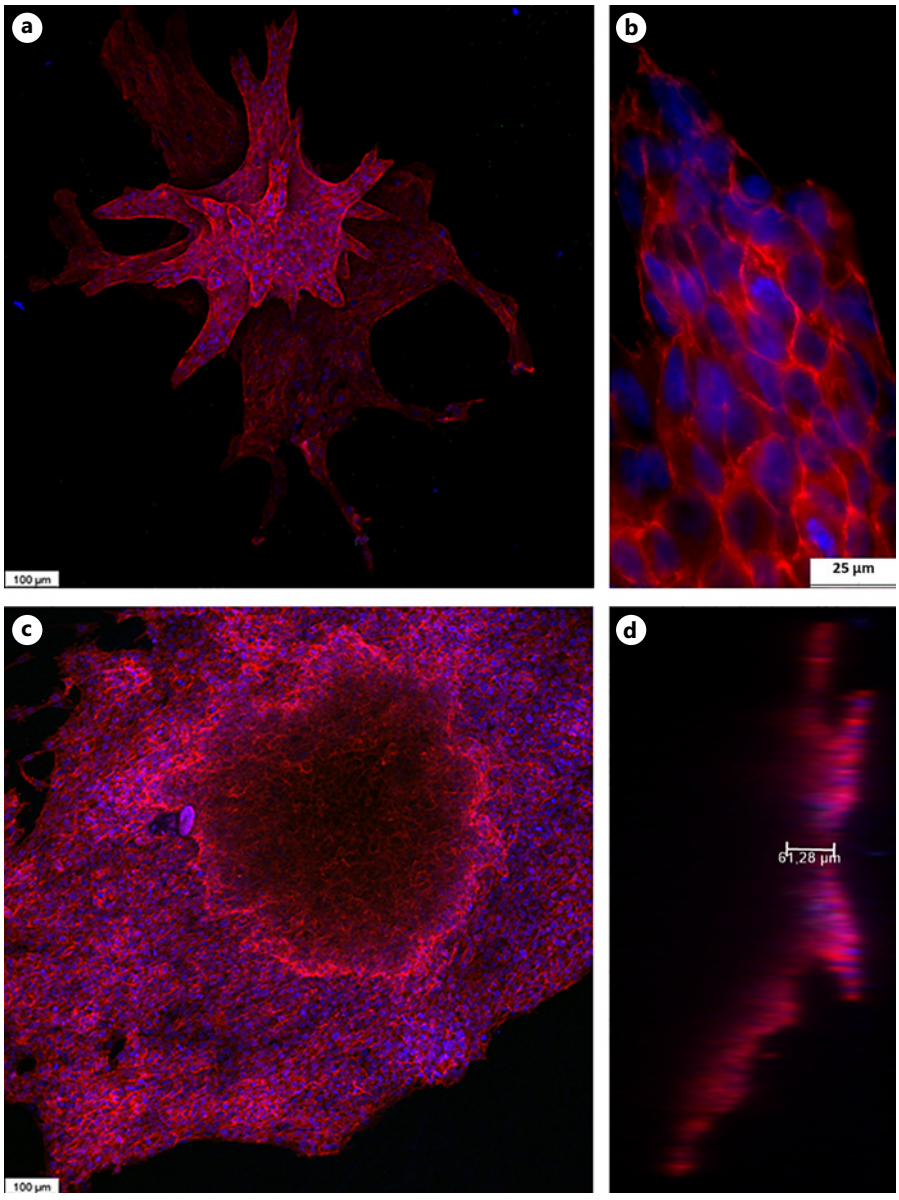

Fig. 9. Microscopic characterization of H1792 spheroids. Spheroids were manufactured and cultured for 1 week. F-actin distribution was examined by phalloidin-rhodamine fluorescence staining (shown in red). Nuclei were stained with DAPI (shown in blue). Samples were observed either with a confocal (**a**, **c**, **d**) or epifluorescence microscope (**b**). The height of the spheroids was determined by confocal microscopy in the Z-axis (**b**). These results are representative of $n = 5$.

abundant matrix deposits. A representative cross section of one of these peripheral cells is shown in Figure 14c, which displayed a characteristic secretory phenotype, as evidenced by the presence of a well-developed Golgi apparatus and RER, as well as mitochondria with pronounced cristae. These cells were surrounded by new deposits of ECM. In addition, several caveolae were observed in its plasma membrane (Fig. 14d).

CAFs induced similar but more noticeable changes in the spheroids. More cellular processes and elongated cells were observed. The cells in the spheroids showed several caveolae (Fig. 15a), and cohesive cells were observed along the spheroids (Fig. 15c). The ECM deposits were more abundant, and in some cases, a new secreted collagen could be seen (Fig. 15c, d), which presented a particular organization with the fibers in parallel to the cellular processes (Fig. 15b, upper asterisk).

In relation to the spheroids generated with H1790 and fibroblasts, we did not find ultrastructural differences in relation to the use of NFs or CAFs. In both cases, we found groups of epithelial cells related by junctional complexes (Fig. 16a) that were smaller and more difficult to find than when H460 cells were used to generate the

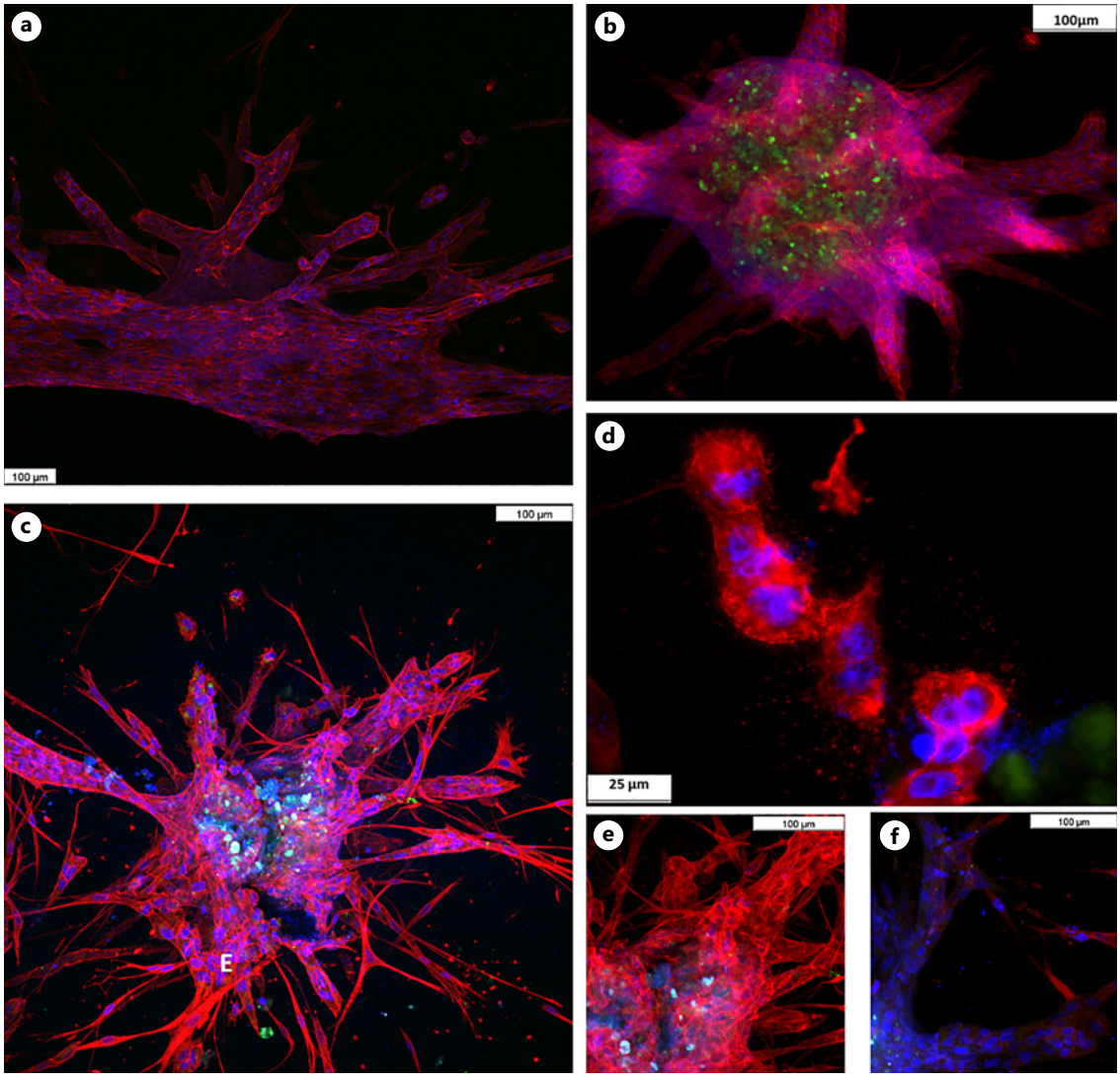

Fig. 10. Microscopic characterization of H1792 + NF spheroids. The spheroids were manufactured and cultured for 1 week. An initial percentage of 50% (**a**, **b**, **d**) or 70% (**c**, **e**, **f**) of stromal cells was used. F-actin distribution was examined by fluorescence staining with phalloidin-rhodamine (shown in red). Pankeratin expression was visualized by immunofluorescence staining (shown in green). Nuclei were stained with DAPI (shown in blue). Samples were observed either with a confocal (**a–c**) or epifluorescence microscope (**d–f**). These results are representative of $n = 5$.

spheroids. We found abundant branches formed by tubular organized epithelial cells as it was observed in transversal sections. In some cases, we could observe cell prolongations of fibroblastic cells in the center of these tubes (Fig. 16b). Around (Fig. 16c) and in front (Fig. 16d) of these branches, we found abundant extensions of fibroblasts with characteristic organelles and a well-developed cytoskeleton surrounded by abundant ECM, presumably secreted by them. We were also able to observe a large number of caveolae in the tumor cells (Fig. 16c).

Relative Gene Expression Analysis of EMT-Related Makers

Finally, to evaluate the EMT, we performed a gene expression analysis of three well-known genes involved in this process: CDH1, CDH2, and VIM. For this purpose, spheroids were harvested after 1 week of culture, total RNA was extracted, and real-time reverse transcriptase polymerase chain reaction was used to analyze the relative levels of gene expression. Glyceraldehyde 3-phosphate dehydrogenase was chosen as the endogenous control and H460 or H1792 spheroids as the control group.

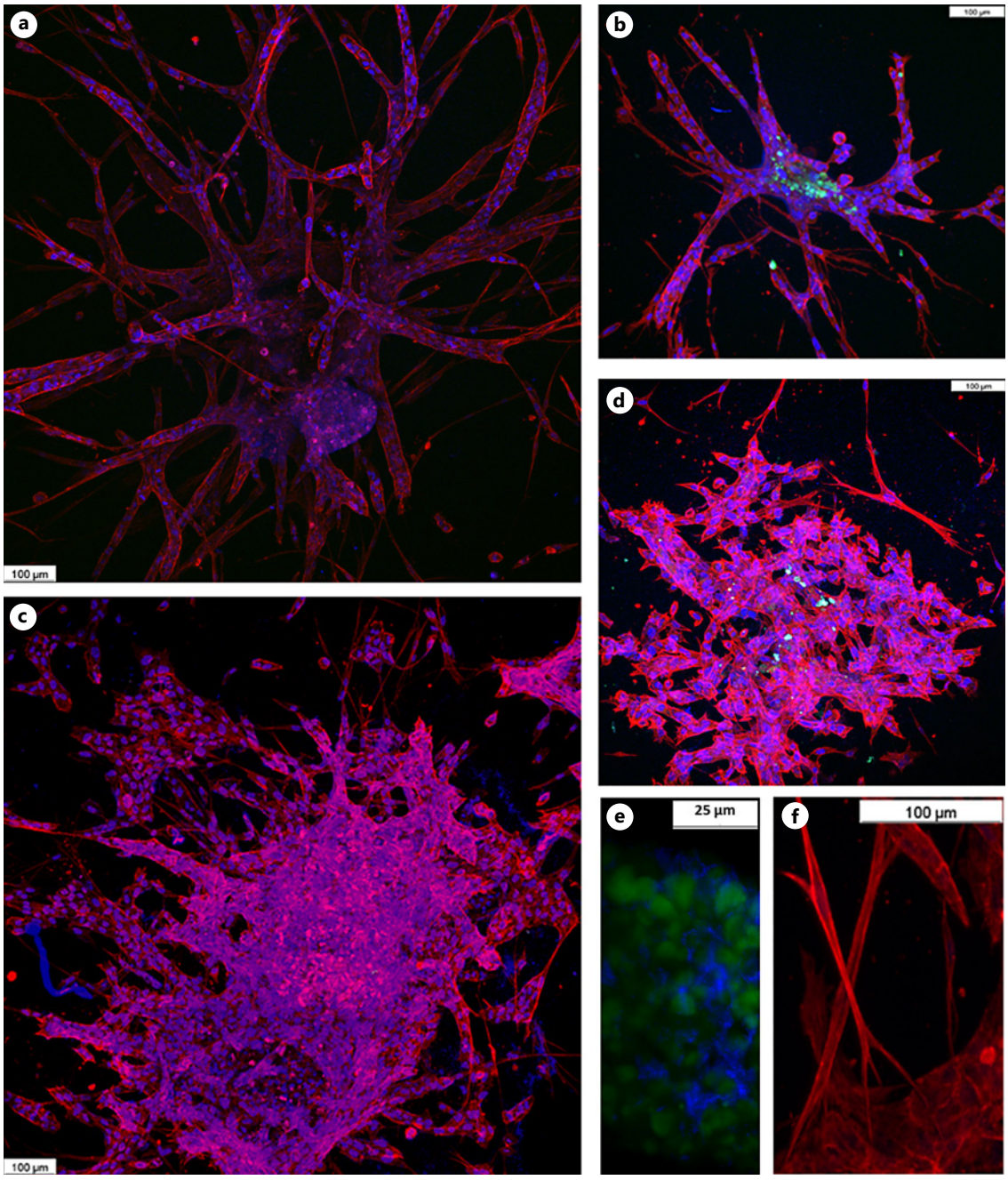

Fig. 11. Microscopic characterization of H1792 + CAF spheroids. The spheroids were manufactured and cultured for 1 week. An initial percentage of 50% (**a**, **b**) or 70% (**c–f**) of stromal cells was used. F-actin distribution was examined by fluorescence staining with phalloidin-rhodamine (shown in red). Pankeratin expression was visualized by immunofluorescence staining (shown in green). Nuclei were stained with DAPI (shown in blue). Samples were observed either with a confocal (**a–d**) or epifluorescence microscope (**e**, **f**). These results are representative of $n = 5$.

In all the spheroids analyzed, stromal cells decreased the relative expression of CDH1 compared to the control group (Fig. 17a). CDH2 expression increased in NF or CAF spheroids, reaching significance in those spheroids containing 70% of stromal cells (NFs or CAFs, Fig. 17b). A similar trend was observed for VIM, in which expression levels reached a maximum in the 70% NF or CAF spheroids (Fig. 17c).

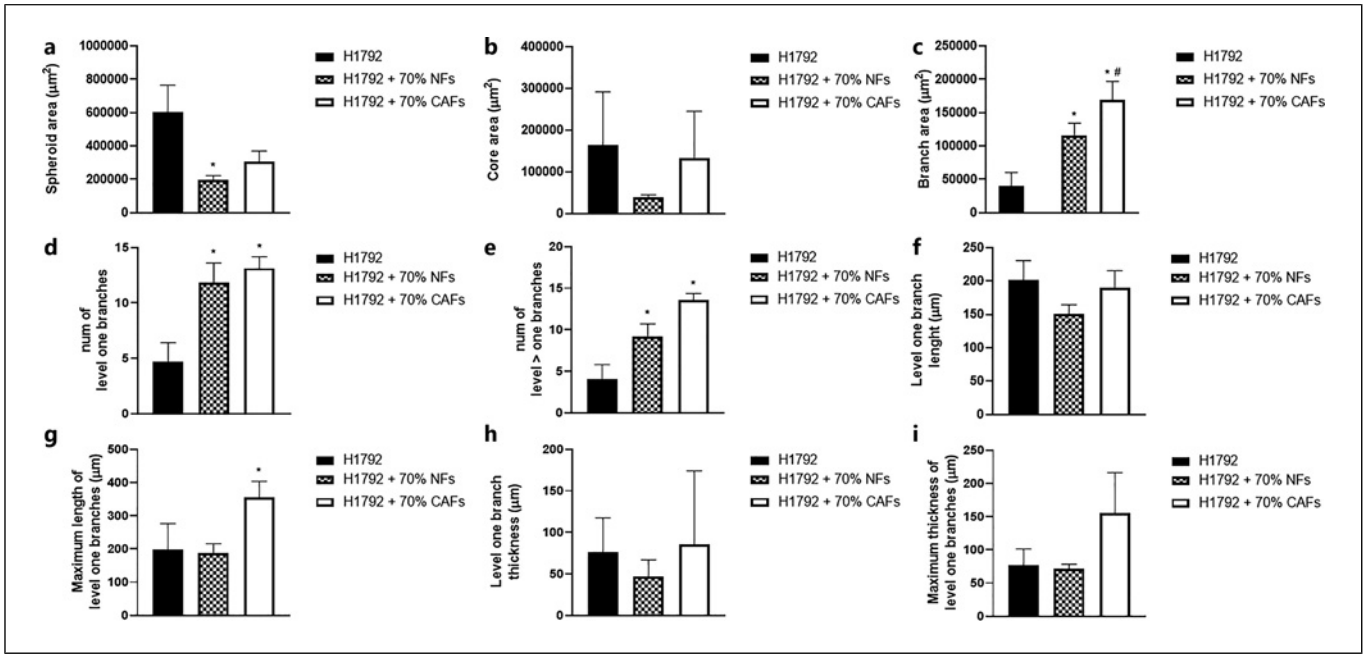

Fig. 12. a–i Morphometric evaluation of H1792 spheroids. Spheroids were manufactured with or without stromal cells (NFs or CAFs) and cultured for 1 week. Morphometric evaluation was done. The results are represented as the mean ± SD of $n = 5$ independent experiments. Each condition was evaluated in 3–6 replicates from three independent observers in a blind manner. *$p < 0.05$ compared to H460 without stromal cell spheroids. #$p < 0.05$ compared to H460 + NF spheroids. SD, standard deviation.

Discussion

Lung cancer is considered one of the malignant neoplasms with the highest incidence and mortality rates, with more than 2,000,000 new cases and 1,800,000 deaths per year in 2020 [25], which indicates the lethality of this type of tumor despite advances in diagnosis, treatment, and prevention. However, different subdivisions of lung cancer are known, which is indicative of different patterns that condition tumor development [26]. Disease progression is determined by specific interactions with the TME that, in turn, induce EMT and are responsible for the great capacity for dissemination and the acquisition of resistance that characterizes this type of cancer.

A goal of future medicine is to achieve personalized medicine [27]. This means changing from general to specific treatments, tailored to the specific pathological characteristics of each patient. In recent years, research groups have been working to elucidate the distinctive mechanisms of each type of tumor [28]. To enable this therapeutic strategy, we need to be able to reproduce in vitro the characteristics of each patient's tumor. To stablish this basis, researchers are striving to develop three-dimensional models that encompass as many elements of the TME as possible, overcoming the limitations of 2D cultures [29, 30]. In our case, we embedded tumor epithelial cells in a type I collagen matrix and cultured them with different proportions of other TME cells, such as CAFs. The aim of generating this model is to investigate the mechanisms of tumorigenesis and establish an in vitro pharmacological model for the study of new anticancer drugs. Thus, the goals were to establish organoids for each patient, perform an in vitro screening of potential treatments, and administer the most effective one to the patient according to the characteristics of the tumor.

The present study aimed to elucidate the participation of cancer and stromal cells in the growth, organization, and cell migration through the generated scaffold previously reported [19]. We generated spheroids from two different NSCLC cell lines. The H460 cells originated from a large-cell carcinoma, and the H1792 cells from an adenocarcinoma. To simulate the ECM, we employed a matrix composed of type I collagen, which is the main component of the matrix in vivo. Finally, these spheroids contain NFs or CAFs in variable proportions according to standardized conditions [19].

We have designed this research based on four fundamental aspects: (i) we have carried out studies of the

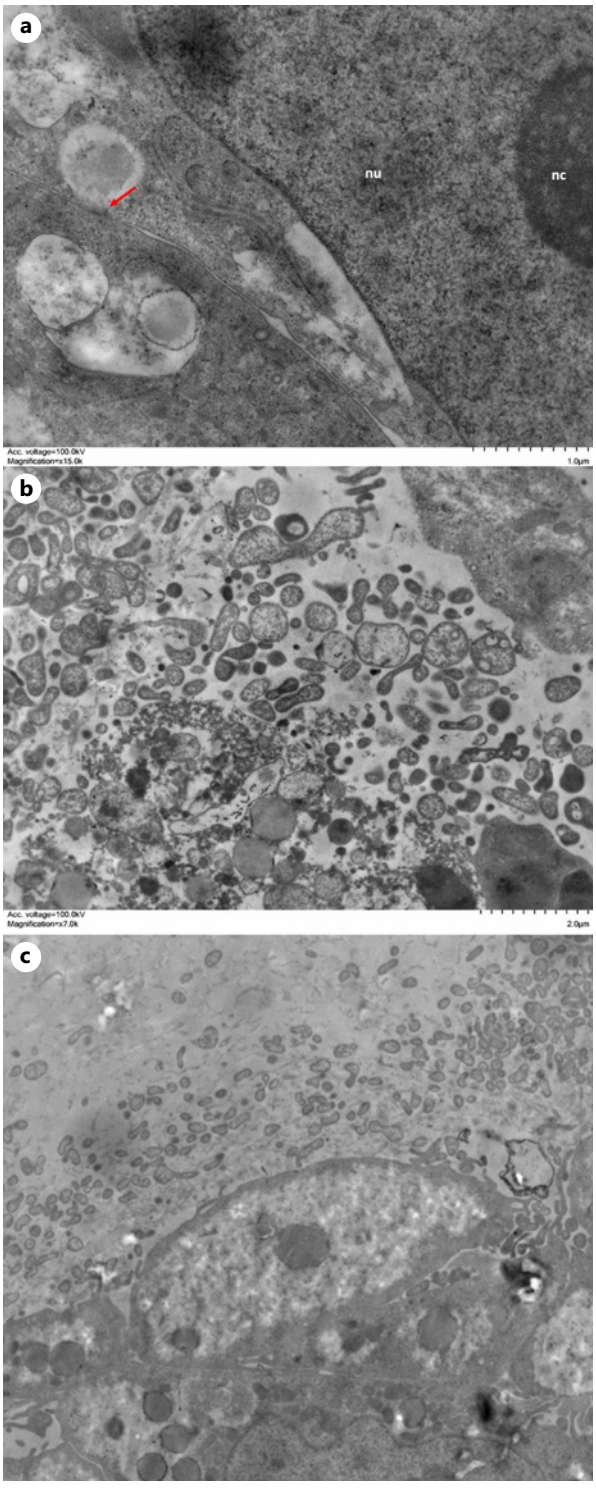

Fig. 13. a–c Ultrastructural features of H460 cell spheroids. H460 spheroids were generated and cultured for 1 week. Samples were analyzed with TEM. Results shown are representative of $n = 5$ experiment performed. nu, nucleus; nc, nucleolus; red arrow, junctional complexes.

microscopic morphology using phase contrast microscopy to evaluate the growth of spheroids in culture. (ii) We have carried out 3D studies of the spheroids using confocal microscopy to study the interactions between the different cells used in the spheroid reorganization process. (iii) We have also evaluated the ultrastructural characteristics of the cells in relation to their position within the spheroid using TEM. (iv) We performed a morphometric analysis of spheroids generated in order to support and quantify the findings after microscopic evaluations of 3D cultures. (v) Finally, we have evaluated the expression of genes involved in the EMT process.

Based on the 3D representations and height measurements obtained by confocal microscopy, we can establish differences and similarities between the study conditions. Regarding the spheroids established from the H460 cell line, we can confirm that they exhibit a great resemblance to those established with the A549 cell line [19]. All conditions show the described structure with well-defined borders. The microscopic and morphometric analysis showed that the addition of the stromal cells implies the increase of the spheroid and core area, as well as the formation of branches. These changes were higher when H460 cells were combined with CAFs instead of NFs. The presence of CAFs not only influenced the growth and branching of the spheroids, but also induced the development of a secretory phenotype in most of the cells that make up the spheroids, which is in line with many of the effects attributed to these cells [11].

Regarding the spheroids manufactured with the H1792 cell line, they present completely different characteristics than those described above, with a different morphology from that of the H460 and A549 cells [19]. This cell type was not organized generating compact structures; rather, they acquired an epithelial organization, generally covering the collagen matrix in which they were embedded and did not present the highly cohesive structures observed in the previous cases. The addition of stromal cells, as in the other cell lines, caused the appearance of branches. However, the structures they adopted prevented their area and height to be quantified. Again, the combination of H1792 cells with stromal (particularly CAFs) induces a profuse ramification of the spheroids. This pattern is compatible with that observed in adenocarcinomas in situ, which usually do not infiltrate the stroma and also maintain an alveolar morphology with cancer cells growing in a single layer along the alveolar septa and serving as a scaffold in a configuration known as "butterfly wings" [31]. Regarding the spheroid area measurements, it must be taken into account that, on the one hand, spheroids formed only by cancer cells tend to form epithelial structures, while those

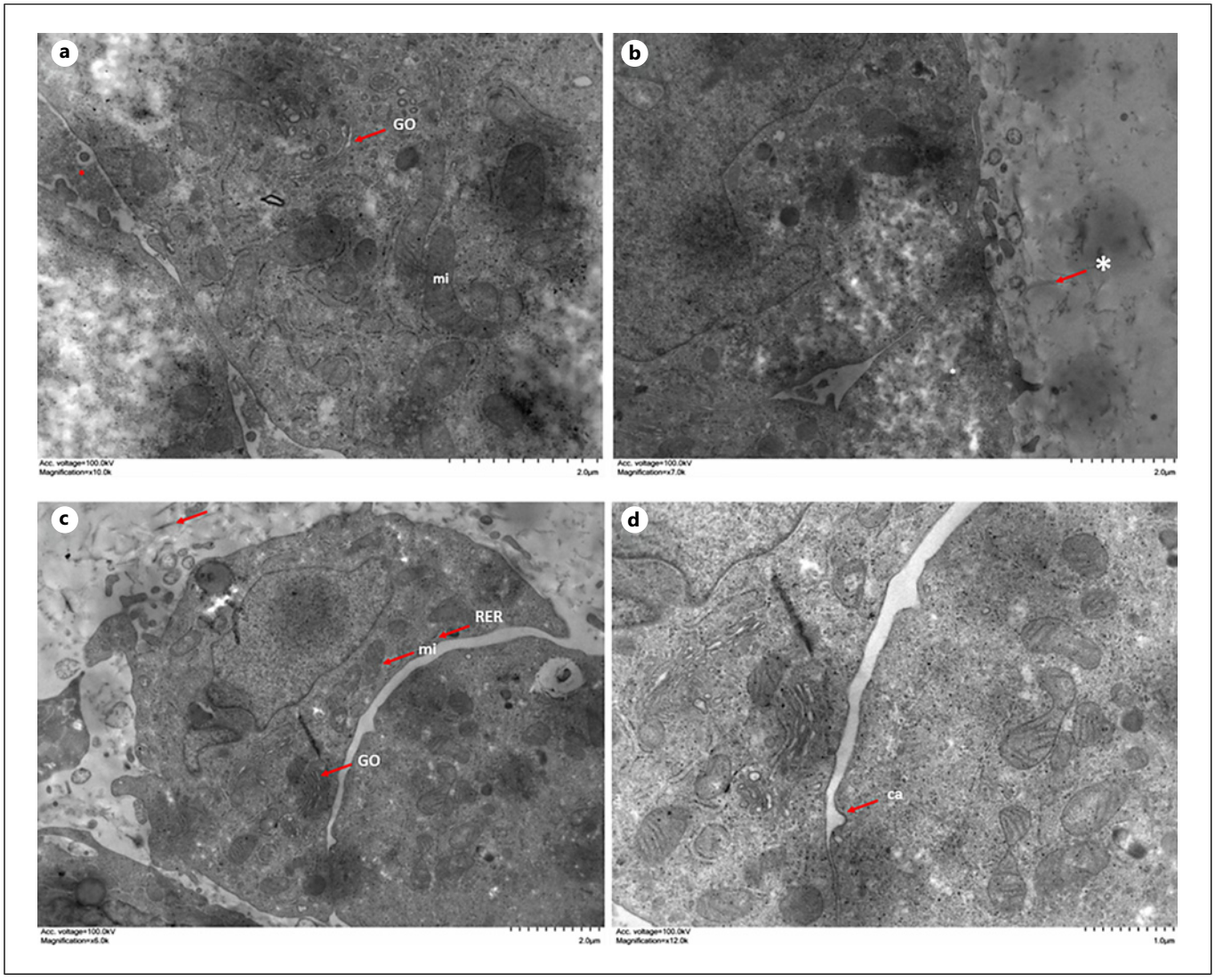

Fig. 14. a–d Ultrastructural features of H460 + NF spheroids. Spheroids were generated and cultured for 1 week. Samples were analyzed with TEM. The results shown are representative of $n = 5$ experiment performed. GO, Golgi apparatus; mi, mitochondria; asterisk, ECM deposits; ca, caveolae.

combined with stromal cells do not show such formations, but rather very ramified structures where the core is difficult to determine, so care must be taken when interpreting these results.

Data from the spheroid areas of H460 cells indicated that these spheroids have a larger size compared to those of A549 cells [19]. Furthermore, studies performed with HCT 116 cell spheroids, a colorectal carcinoma cell line, also showed that lung cell spheroids were larger in size compared to H460 spheroids. Additionally, in the same study, lung spheroids exhibited similar structures to those shown in our study, despite using a different method to generate spheroids [32]. To explain the significant increase in size that we have observed, we consider two possible causes: first, due to the higher proliferation rate exhibited by the H460 cell line (as observed in 2D cultures [33]), which leads to the formation of these structures, and second, by the possible aggregation of multiple small spheroids to form larger structures.

Despite the previous description that the branching structures are formed by epithelial cells, based on pan-keratin expression patterns, it seems that this organized migration is led by the stromal cells. In the images, it can be observed that the leading edge of the branched

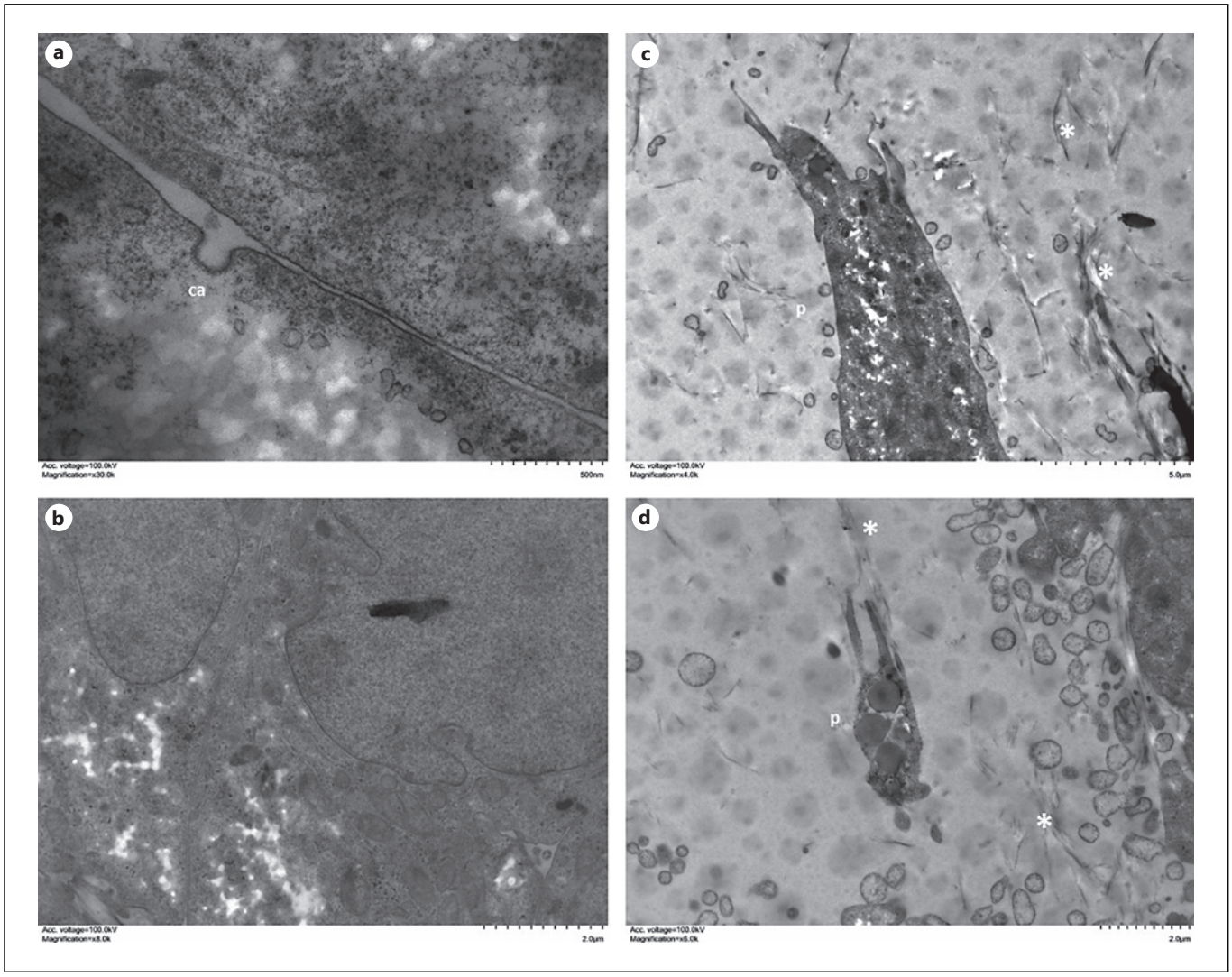

Fig. 15. a–d Ultrastructural features of H460 + CAF spheroids. Spheroids were generated and cultured for 1 week. Samples were analyzed with TEM. The results shown are representative of $n = 5$ experiment performed. Asterisk, ECM deposits; ca, caveolae; p, cellular process.

structure has a clearly fibroblastic, pankeratin-negative morphology (Fig. 4e), probably due to the tendency of stromal cells to migrate toward areas of higher tension [34, 35]. However, it is necessary to carry out biomechanical studies to verify this hypothesis. On the other hand, in some immunofluorescence images, as shown in Figure 6d, although only epithelial cells are present in the spheroid, we did not observe clear expression of pankeratin. We have two hypotheses that try to explain this fact. First, it could be due to the downregulation of certain genes that tumor cells undergo, which is related to the EMT phenomenon [36]. Second, it could be attributed to the use of dry panoramic objectives, which implies a resolution limitation for the technique used; in this case, it would be a problem of detection rather than expression. A more precise histological study is necessary to verify whether the absence of pankeratin may be an artifact due to the need to use panoramic objectives for the morphological characterization of the spheroids.

EMT is a relevant process related to cell migration and tumor dissemination. Relative gene expression studies have shown that the addition of stromal cells to spheroids induced a decrease in CDH1 expression, characteristic of epithelial cells [37, 38]. Additionally, there is a slight increase in CDH2 expression and a greater increase of VIM, characteristic of mesenchymal cells [38].

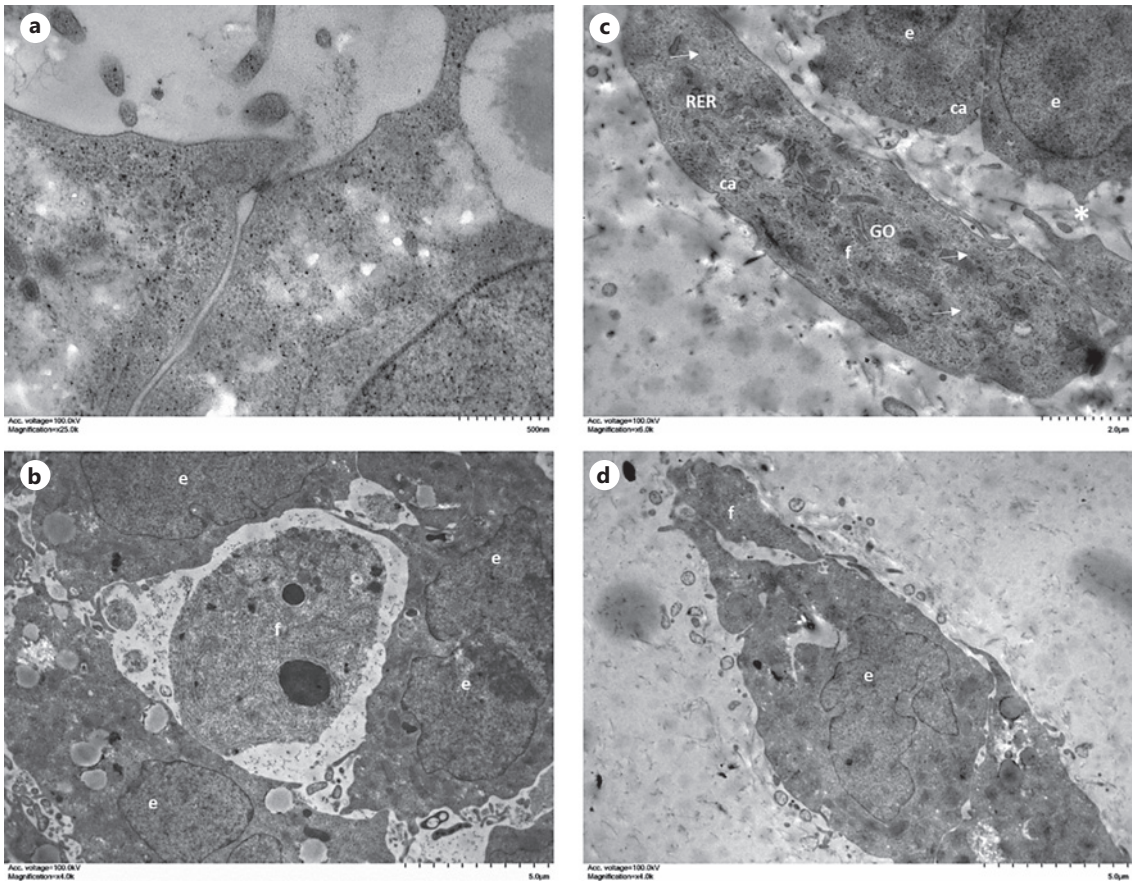

Fig. 16. a–d Ultrastructural features of H1790 + CAF spheroids. Spheroids were generated and cultured for 1 week. Samples were analyzed with TEM. The results shown are representative of $n = 5$ experiment performed. Asterisk, ECM deposits; ca, caveolae; f, fibroblast; e, epithelial cell; GO, Golgi apparatus.

The ultrastructural studies carried out allowed us to detect the presence of secretory phenotypes, as well as the presence of caveolae. Several studies have linked these structures to carcinogenesis [39–41]. Caveolae are multifunctional structures with both structural and functional roles. Thus, genetic alterations that affect their correct function led to the appearance of cellular physiopathology.

With respect to personalized medicine and treatment, time plays a crucial factor. Indeed, the speed of the process to establish spheroids from the patient's cells is crucial for its clinical applicability. The aim was for the process to be efficient, reproducible, and capable of providing timely information to guide personalized treatment decisions. Our model can be generated in just 1 week, which opens the possibility of using it for drug testing before applying any treatment to the patient. Other studies indicate that a 4-week establishment is considered relatively fast, giving our method an advantage over other models [42].

On the other hand, our model did not reproduce all tumor characteristics, which may lead to a substantial loss of information. Other research groups are trying to include different relevant cell types [43], such as endothelial cells or macrophages. Another option would be to include some other component of the ECM besides type I collagen.

In summary, the findings presented herein suggest that the epithelial cancer type influences the patterns of spheroid growth, cell migration, and secretory phenotype of cells in our experimental model. While this model is still in its early stages and requires refinement by controlling cell populations, incorporating endothelial and immune cells, and integrating characteristic elements of the tumor matrix such as type I collagen, we

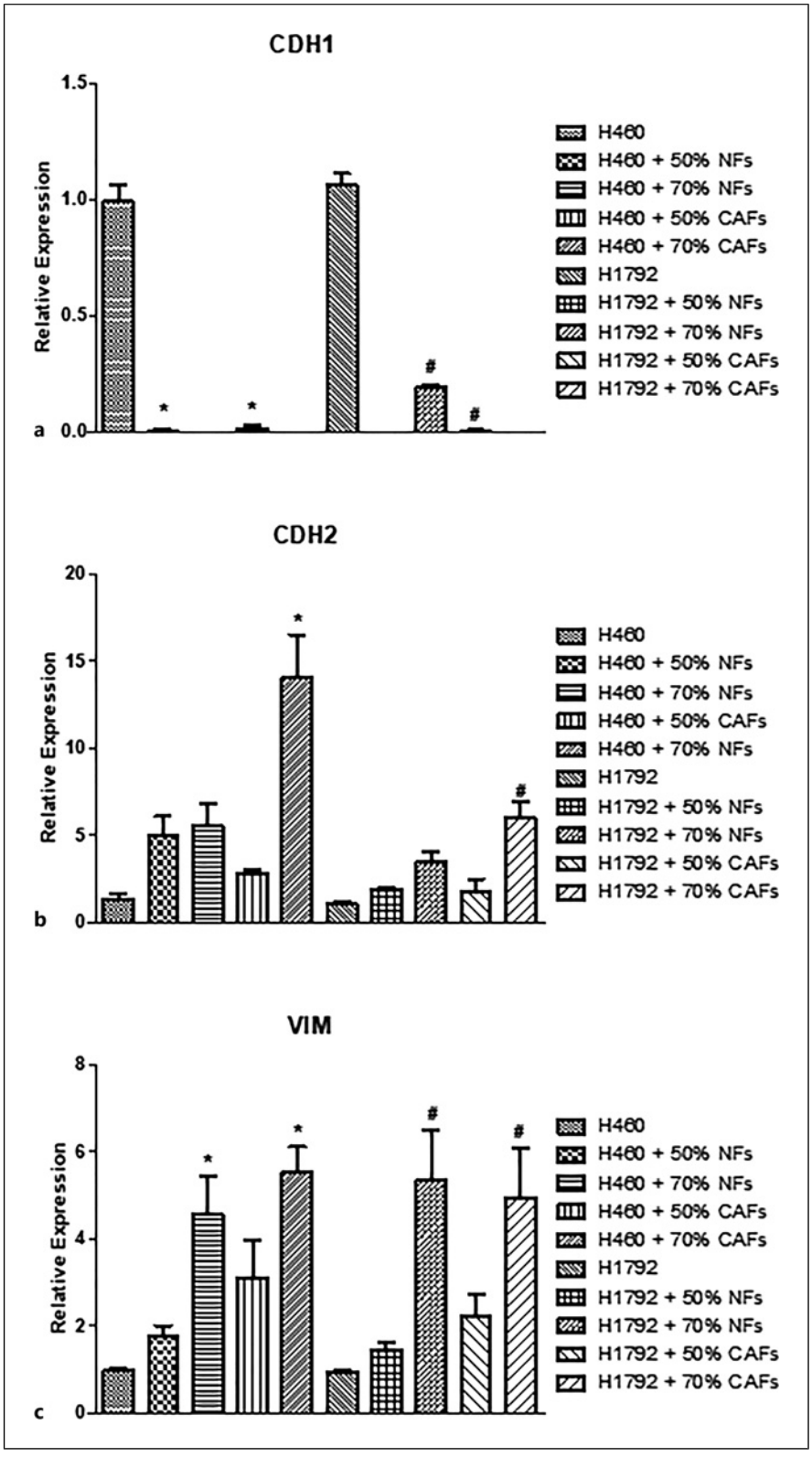

Fig. 17. Relative gene expression of CDH1 (**a**), CDH2 (**b**), and VIM (**c**). Relative gene expression was quantified using real-time RT-PCR. The comparative ΔΔCt method was employed to determine the relative changes. The GAPDH gene served as the housekeeping gene. The results are the mean ± SD of $n = 5$ independent experiments. *$p < 0.05$ compared to H460 without stromal cell spheroids. #$p < 0.05$ compared to H1792 without stromal cell spheroids. RT-PCR, reverse transcriptase polymerase chain reaction; GAPDH, glyceraldehyde 3-phosphate dehydrogenase; SD, standard deviation; NFs, normal fibroblasts; CAFs, cancer-associated fibroblasts.

believe it holds promise as a valuable tool for investigating interactions within the TME. Furthermore, it has the potential to serve as a novel platform for pharmacological screening of antitumor drugs.

Acknowledgments

We want to thank Antonio Ibáñez, from the UCIM (Central Medicine Research Unit, University of Valencia, Spain) for the support with the confocal microscopy experiments, and the staff of SCSIE (Central Support Service for Experimental Research, University of Valencia, Spain) for their help with the electron microscopy experiments.

Statement of Ethics

This study protocol was reviewed and approved by the Ethics Committee of the Hospital La Ribera, Valencia, Spain, approval on October 05, 2023, and written informed consent was obtained from any adults participating in this study.

Conflict of Interest Statement

The authors have no conflicts of interest to declare.

Funding Sources

This work was supported by grant PID2019-106099RB-C42 (MM) from the Ministry of Economy and Competitiveness of the Spanish Government and by grant AECC (Asociación Española Contra el Cáncer). CIBERER is financed by the VI National R&D&I Plan, Iniciativa Ingenio 2010, Consolider Program, CIBER Actions, and the Instituto de Salud Carlos III, with the assistance of the European Regional Development Fund.

Author Contributions

I.M.-G.: formal analysis, investigation, methodology, and visualization. L.B.-B.: formal analysis, investigation, methodology, visualization, and writing original draft. L.M.: methodology, visualization, and supervision. M.S.-T.: funding and writing – review and editing. M.L.-M.: methodology. J.M.G. and A.C.: resources. C.C.: funding and resources. M.M.: conceptualization, formal analysis, funding, project administration, supervision, visualization, and writing original draft.

Data Availability Statement

All data are included in the manuscript and supplementary material. Further inquiries can be directed to the corresponding author.

References

1 Stone E, Dodd RH, Marshall H, Bonevski B, Rankin NM. Lung cancer screening: the hidden public health emergency. Public Health Res Pract. 2023;33(1):3312302. https://doi.org/10.17061/phrp3312302
2 Nooreldeen R, Bach H. Current and future development in lung cancer diagnosis. Int J Mol Sci. 2021;22(16):8661. https://doi.org/10.3390/ijms22168661
3 Billah S, Stewart J, Staerkel G, Chen S, Gong Y, Guo M. EGFR and KRAS mutations in lung carcinoma: molecular testing by using cytology specimens. Cancer Cytopathol. 2011;119(2):111–7. https://doi.org/10.1002/cncy.20151
4 Sequist LV, Waltman BA, Dias-Santagata D, Digumarthy S, Turke AB, Fidias P, et al. Genotypic and histological evolution of lung cancers acquiring resistance to EGFR inhibitors. Sci Transl Med. 2011;3(75):75ra26. https://doi.org/10.1126/scitranslmed.3002003
5 Altorki NK, Markowitz GJ, Gao D, Port JL, Saxena A, Stiles B, et al. The lung microenvironment: an important regulator of tumour growth and metastasis. Nat Rev Cancer. 2019;19(1):9–31. https://doi.org/10.1038/s41568-018-0081-9
6 Xiao Y, Yu D. Tumor microenvironment as a therapeutic target in cancer. Pharmacol Ther. 2021;221:107753. https://doi.org/10.1016/j.pharmthera.2020.107753
7 Runa F, Hamalian S, Meade K, Shisgal P, Gray PC, Kelber JA. Tumor microenvironment heterogeneity: challenges and opportunities. Curr Mol Biol Rep. 2017;3(4):218–29. https://doi.org/10.1007/s40610-017-0073-7
8 Cox TR. The matrix in cancer. Nat Rev Cancer. 2021;21(4):217–38. https://doi.org/10.1038/s41568-020-00329-7
9 Pawlina W, Ross MH. Histology: a text and atlas: with correlated cell and molecular biology. 8th ed. Philadelphia, USA: Lippincott Williams and Wilkins; 2018.
10 Hackett TL, Osei ET. Modeling extracellular matrix-cell interactions in lung repair and chronic disease. Cells. 2021;10(8):2145. https://doi.org/10.3390/cells10082145
11 Wong KY, Cheung AH, Chen B, Chan WN, Yu J, Lo KW, et al. Cancer-associated fibroblasts in non-small cell lung cancer: from molecular mechanisms to clinical implications. Int J Cancer. 2022;151(8):1195–215. https://doi.org/10.1002/ijc.34127
12 Mittal V. Epithelial mesenchymal transition in tumor metastasis. Annu Rev Pathol. 2018;13(1):395–412. https://doi.org/10.1146/annurev-pathol-020117-043854
13 Granat LM, Kambhampati O, Klosek S, Niedzwecki B, Parsa K, Zhang D. The promises and challenges of patient-derived tumor organoids in drug development and precision oncology. Exp Med. 2019;2(3):150–61. https://doi.org/10.1002/ame2.12077
14 Zhou J, Su J, Fu X, Zheng L, Yin Z. Microfluidic device for primary tumor spheroid isolation. Exp Hematol Oncol. 2017;6(1):22. https://doi.org/10.1186/s40164-017-0084-3
15 Caponigro G, Sellers WR. Advances in the preclinical testing of cancer therapeutic hypotheses. Nat Rev Drug Discov. 2011;10(3):179–87. https://doi.org/10.1038/nrd3385
16 Hoyte L, Kaur J, Buchan AM. Lost in translation: taking neuroprotection from animal models to clinical trials. Exp Neurol. 2004;188(2):200–4. https://doi.org/10.1016/j.expneurol.2004.05.008
17 Habanjar O, Diab-Assaf M, Caldefie-Chezet F, Delort L. 3D Cell culture systems: tumor application, advantages, and disadvantages. Int J Mol Sci. 2021;22(22):12200. https://doi.org/10.3390/ijms222212200
18 Chae YK, Chang S, Ko T, Anker J, Agte S, Iams W, et al. Epithelial-mesenchymal transition (EMT) signature is inversely associated with t-cell infiltration in non-small cell lung cancer (NSCLC). Sci Rep. 2018;8(1):2918. https://doi.org/10.1038/s41598-018-21061-1

19 Monleón-Guinot I, Milian L, Martínez-Vallejo P, Sancho-Tello M, Llop-Miguel M, Galbis JM, et al. Morphological characterization of human lung cancer organoids cultured in type i collagen hydrogels: a histological approach. Int J Mol Sci. 2023;24(12):10131. https://doi.org/10.3390/ijms241210131
20 Salvador-Clavell R, Martín de Llano JJ, Milián L, Oliver M, Mata M, Carda C, et al. Chondrogenic potential of human dental pulp stem cells cultured as microtissues. Stem Cells Int. 2021;2021:7843798. https://doi.org/10.1155/2021/7843798
21 Milián L, Monleón-Guinot I, Sancho-Tello M, Galbis JM, Cremades A, Almenar-Ordaz M, et al. In vitro effect of Δ9-tetrahydrocannabinol and cannabidiol on cancer-associated fibroblasts isolated from lung cancer. Int J Mol Sci. 2022;23(12):6766. https://doi.org/10.3390/ijms23126766
22 Oliver-Ferrándiz M, Milián L, Sancho-Tello M, Martín de Llano JJ, Gisbert Roca F, Martínez-Ramos C, et al. Alginate-agarose hydrogels improve the in vitro differentiation of human dental pulp stem cells in chondrocytes. A histological study. Biomedicines. 2021;9(7):834. https://doi.org/10.3390/biomedicines9070834
23 Caruso M, Huang S, Mourao L, Scheele CLGJ. A mammary organoid model to study branching morphogenesis. Front Physiol. 2022;13:826107. https://doi.org/10.3389/fphys.2022.826107
24 Bankhead P, Loughrey MB, Fernández JA, Dombrowski Y, McArt DG, Dunne PD, et al. QuPath: open source software for digital pathology image analysis. Sci Rep. 2017;7(1):16878. https://doi.org/10.1038/s41598-017-17204-5
25 Global cancer observatory. Available from: https://gco.iarc.fr/ (accessed on 04 06, 2023).
26 Fois SS, Paliogiannis P, Zinellu A, Fois AG, Cossu A, Palmieri G. Molecular epidemiology of the main druggable genetic alterations in non-small cell lung cancer. Int J Mol Sci. 2021;22(2):612. https://doi.org/10.3390/ijms22020612
27 Jiang W, Cai G, Hu PC, Wang Y. Personalized medicine in non-small cell lung cancer: a Review from a pharmacogenomics perspective. Acta Pharm Sin B. 2018;8(4):530–8. https://doi.org/10.1016/j.apsb.2018.04.005
28 Braig ZV. Personalized medicine: from diagnostic to adaptive. Biomed J. 2022;45(1):132–42. https://doi.org/10.1016/j.bj.2019.05.004
29 Ma HC, Zhu YJ, Zhou R, Yu YY, Xiao ZZ, Zhang HB. Lung cancer organoids, a promising model still with long way to go. Crit Rev Oncol Hematol. 2022;171:103610. https://doi.org/10.1016/j.critrevonc.2022.103610
30 Zimmermann M, Box C, Eccles SA. Two-dimensional vs. three-dimensional in vitro tumor migration and invasion assays. Methods Mol Biol. 2013;986:227–52. https://doi.org/10.1007/978-1-62703-311-4_15
31 Mitchell RN, KumarV AAK, Aster JC. Compendio de Robbins y Cotran. Patología estructural y funcional. 9th ed. Barcelona, Spain: Elsevier; 2017.
32 Kulesza J, Pawłowska M, Augustin E. The influence of antitumor unsymmetrical bisacridines on 3d cancer spheroids growth and viability. Molecules. 2021;26(20):6262. https://doi.org/10.3390/molecules26206262
33 Milian L, Mata M, Alcacer J, Oliver M, Sancho-Tello M, Martín de Llano JJ, et al. Cannabinoid receptor expression in non-small cell lung cancer. Effectiveness of tetrahydrocannabinol and cannabidiol inhibiting cell proliferation and epithelial-mesenchymal transition in vitro. PLoS One. 2020;15(2):e0228909. https://doi.org/10.1371/journal.pone.0228909
34 Asif PJ, Longobardi C, Hahne M, Medema JP. The role of cancer-associated fibroblasts in cancer invasion and metastasis. Cancers. 2021;13(18):4720. https://doi.org/10.3390/cancers13184720
35 Singh V, Lamaze C. Membrane tension buffering by caveolae: a role in cancer? Cancer Metastasis Rev. 2020;39(2):505–17. https://doi.org/10.1007/s10555-020-09899-2
36 Yang S, Liu Y, Li MY, Ng CSH, Yang SL, Wang S, et al. FOXP3 promotes tumor growth and metastasis by activating Wnt/β-catenin signaling pathway and EMT in non-small cell lung cancer. Mol Cancer. 2017;16(1):124. https://doi.org/10.1186/s12943-017-0700-1
37 Lambert AW, Pattabiraman DR, Weinberg RA. Emerging biological principles of metastasis. Cell. 2017;168(4):670–91. https://doi.org/10.1016/j.cell.2016.11.037
38 Ziegler E, Hansen MT, Haase M, Emons G, Gründker C. Generation of McF-7 cells with aggressive metastatic potential in vitro and in vivo. Breast Cancer Res Treat. 2014;148(2):269–77. https://doi.org/10.1007/s10549-014-3159-4
39 Lamaze C, Torrino S. Caveolae and cancer: a new mechanical perspective. Biomed J. 2015;38(5):367–79. https://doi.org/10.4103/2319-4170.164229
40 Low JY, Laiho M. Caveolae-associated molecules, tumor stroma, and cancer drug resistance: current findings and future perspectives. Cancers. 2022;14(3):589. https://doi.org/10.3390/cancers14030589
41 Martinez-Outschoorn UE, Sotgia F, Lisanti MP. Caveolae and signalling in cancer. Nat Rev Cancer. 2015;15(4):225–37. https://doi.org/10.1038/nrc3915
42 Kim M, Mun H, Sung CO, Cho EJ, Jeon HJ, Chun SM, et al. Patient-derived lung cancer organoids as in vitro cancer models for therapeutic screening. Nat Commun. 2019;10(1):3991. https://doi.org/10.1038/s41467-019-11867-6
43 Choi YM, Lee H, Ann M, Song M, Rheey J, Jang J. 3D Bioprinted vascularized lung cancer organoid models with underlying disease capable of more precise drug evaluation. Biofabrication. 2023;15(3):034104. https://doi.org/10.1088/1758-5090/acd95f